Materials Advances

ROYAL SOCIETY OF CHEMISTRY

REVIEW

View Article Online
View Journal | View Issue

Cite this: *Mater. Adv.*, 2023, 4, 4272

Graphene quantum dots: synthesis, characterization, and application in wastewater treatment: a review

Peyman Gozali Balkanloo, Kolsum Mohammad Sharifi and Ahmad Poursattar Marjani *

Graphene quantum dots (GQDs) are nanoscale particles of graphene, typically having a diameter of less than 20 nm. The unique attributes of GQDs include low toxicity, good solubility, tunable photoluminescence (PL), biocompatibility, and photo-induced electron transfer. GQDs can be produced using hydrothermal reactions, laser ablation, microwave radiation, and electrochemical oxidation. These procedures for producing GQDs involve various chemical reactions, including carbonization, oxidation, pyrolysis, and polymerization. Due to their small particle sizes, GQDs possess strong tunable fluorescent properties and exhibit high photo-luminescence emissions. GQDs have been acknowledged as appropriate for various applications, such as eliminating pollutants and organic dyes through catalysis, absorbing heavy metals, and purifying microbial contamination through filtration. However, challenges encountered during the development of GQDs for environmental applications include generating high-quality QDs and devising large-scale synthetic procedures that ensure reproducible size distribution. A need exists for theoretical and practical research on the development of novel methods that allow high yields and easy purification of GQDs to be achieved. In this article, the characteristics of GQDs in terms of their chemical and physical attributes are analyzed. The raw materials and techniques employed in the manufacturing process of GQDs are also discussed, along with their stability. Additionally, the potential applications of GQDs in treating wastewater are explored.

Received 6th July 2023,
Accepted 7th August 2023

DOI: 10.1039/d3ma00372h

rsc.li/materials-advances

Department of Organic Chemistry, Faculty of Chemistry, Urmia University, Urmia, Iran. E-mail: a.poursattar@urmia.ac.ir, a.poursattar@gmail.com

Peyman Gozali Balkanloo

Peyman Gozali Balkanloo is currently pursuing his PhD in organic chemistry at Urmia University under the supervision of Professor Ahmad Poursattar Marjani. Peyman's academic journey began at the University of Mohaghegh Ardabili, where he completed his bachelor's degree in applied chemistry. Motivated by his desire to delve deeper into the world of nanoscience, Peyman pursued a master's degree at Urmia University. His research in nanochemistry has led to groundbreaking discoveries in the field, resulting in the publication of several academic papers in renowned journals. His research interests encompass various areas such as membrane separation processes, hydrogels' application in agriculture, and Li-ion batteries.

Kolsum Mohammad Sharifi

Kolsum Mohammad Sharifi obtained her bachelor's degree by securing the top position at Payame noor Mahabad University, Iran. Currently, she is pursuing a master's degree under the supervision of Professor Ahmad Poursattar Marjani in the Faculty of Chemistry at Urmia University, Iran. Her area of focus lies in polymer nanotechnology, which she is actively studying and researching.

Introduction

During the last two decades, a great deal of attention has been focused on the optoelectronic properties of nanostructured semiconductors or quantum dots (QDs) as many fundamental properties are size dependent in the nanometer range.[1] Since the discovery of graphene in 2004, metal-free carbon-based QDs, *i.e.*, carbon QDs (CQDs), GQDs, and graphitic-carbon nitride QDs (g-CNQDs), have drawn considerable attention as promising candidates as they have the potential to replace the conventional metallic QDs. Carbon-based QDs not only possess good physicochemical properties of metallic QDs like excellent stability and tunable fluorescence, but also exhibit unique merits such as easy synthesis, excellent biocompatibility, and nontoxicity.[2] GQDs, one of the recently discovered carbon-based nanomaterials, are derived from two-dimensional graphene, which limits electronic transport in all three spatial dimensions.[3,4] GQDs are small enough to confine excitons. They have a diameter of less than 20 nanometers and have a non-zero band gap that becomes bright when stimulated.[4] Compared with carbon nanodots, GQDs have good chemical and physical attributes, namely, a greater length-to-diameter ratio, higher surface area, and better surface bonding through the double π–π network due to their graphene layer structure.[5] Additionally, GQDs exhibit an attractive property called photoluminescence (PL), which was reported by Pan *et al.* and attributed to quantum confinement.[6]

When ideal graphene is transformed into a GQD with a semi-dimension size, the band gap becomes adjustable. The precise structure of GQDs depends on the synthesis and doping performed to adjust the band gap. Mahasin *et al.* have conducted a comprehensive theoretical analysis to determine the influence of zigzag edges on the photoluminescent (PL) properties of graphene quantum dots (GQDs) with different sizes. This investigation aimed to understand how their behavior changes in terms of wavelength dispersion as their diameters range from approximately 0.46 to 2.31 nm, spanning from ultraviolet (UV) to infrared PL dispersion. The relationship between the band gap distance and GQD size is such that they are inversely proportional. This means that as the size of the GQD decreases, the band gap distance increases.[7] By manipulating the size and surface chemical groups of GQDs, it is possible to regulate their band gap energy within the range of 0 to 6 electron volts.[8]

GQDs have zero dimensions and possess two fundamental characteristics of edge effects and quantum confinement.[9,10] The quantum confinement mechanism present in GQDs has opened up avenues for utilizing their unique electrical, optical, and structural characteristics that are not readily available in other nanomaterials.[11] GQDs with functionalized edges comprising epoxy, carboxyl, hydroxyl, and carbonyl groups can interact with biological molecules like enzymes, proteins, or antibodies. GQDs have been successfully conjugated to antibody and DNA molecules through amide coupling, which is useful for the fabrication of high-sensitivity nanomaterials and diagnostic tools.[12] GQDs have a crystal lattice structure that resembles a honeycomb, with carbon atoms forming six-membered rings. This arrangement gives rise to the sp^2-hybridized characteristics of GQDs and allows for electron delocalization in the π-orbitals. These properties endow GQDs with their distinct optical and electrical features, which determine the shape of their edges (zigzag or armchair) and influence their PL behavior.[11] Furthermore, GQDs have important properties such as low toxicity, good solubility, stable fluorescence, chemical inertness, and surface grafting (Fig. 1). GQDs have remarkable quantum properties, which is why they have been studied in biological imaging, light-emitting diodes, photoelectrocatalysis, drug carrier sensors, and pollutant absorption.[13–17] One of the most attractive features of GQDs is their abundance as carbon materials, which can be equipped with functional groups at their edges. This feature makes them more desirable than mineral QDs.[4] GQDs exhibit significant behavior that can be used as antimicrobial agents. For example, the modification of GQD properties through doping was first studied in 2012 by Zhao *et al.*, which included nitrogen as a dopant in GQDs.[13]

Ahmad Poursattar Marjani

Ahmad Poursattar Marjani obtained his MSc and PhD in organic chemistry from Urmia University. Currently, he holds the position of a Professor of Organic Chemistry at Urmia University's Faculty of Chemistry. His research focuses on creating novel approaches for synthesizing different types of heterocyclic compounds, nanomaterials, and nanocatalysts.

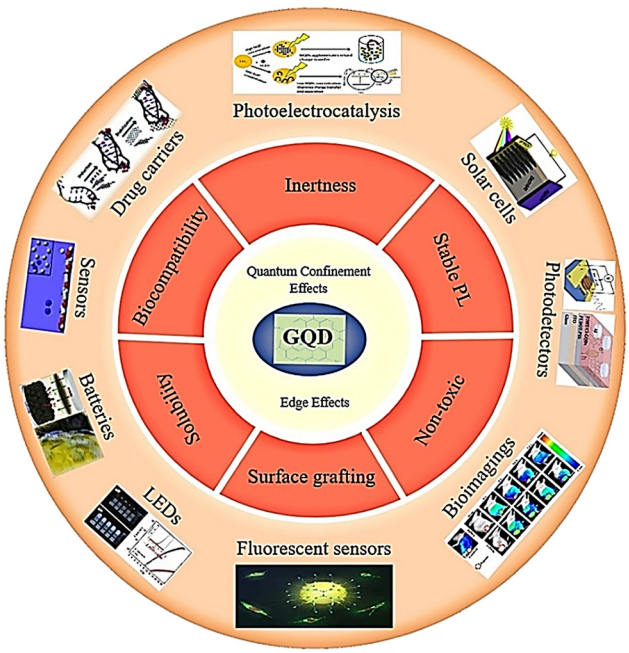

Fig. 1 Properties and applications of GQDs.

The color of GQDs would turn into a light blue fluorescence upon exposure to UV-light irradiation. GQDs with a size of less than 15 nm are obtained through low-carbonization, resulting in blue luminescence. GQDs contain abundant sp^2 structures and oxygen functional groups. The wavelength of GQD dispersion is independent of stimulation, and the sp^2 surface state in GQDs should be uniform.[18]

Numerous carbon sources have been utilized in the production of GQDs, and it is widely recognized that the fluorescence properties of GQDs are influenced by the choice of the precursor. Precursors that contain a significant amount of sp^2 carbon domains are ideal for creating GQDs.[19] Citric acid precursors have been used to prepare GQDs with PL features forming large graphene sheets.[20]

Therefore, GQDs can potentially be used for heavy metal detection in water,[21–23] organic and mineral pollutant removal,[24–26] and photocatalytic degradation[27] due to their high electron mobility, easy transfer, and adjustable light absorption.[27] GQDs are semiconductor nanoparticles that are entirely made up of carbonaceous materials;[3] therefore, GQDs can be applied in analytical nanosciences,[28] sensor fabrication due to their biocompatibility and chemical inertness,[6] as well as in nanotechnology[29] applications. They can also be used for heavy metal detection,[30] photovoltaic device sensitizers,[31] biological molecule detection,[32] photocatalytic processes,[33] energy storage, and production.[34]

A study has been carried out on converting biomass waste into GQDs through easy, scalable, and low-cost routes, focusing on discovering their applications in energy conversion and storage for achieving goals and solving problems of biological waste recycling.[35] In another study, GQDs were synthesized to construct an electrochemical safety sensor for detecting food toxins, aflatoxin B_1 (AFB_1).[36] GQDs are utilized as fluorescence sensors to find ethion in food samples, and their potential is further enhanced by their extensive surface area, ability to integrate with other materials, promote charge transfer and transport, and diverse range of applications in energy storage. GQDs are also effective as light-sensitive sensors in optical detectors due to their strong light absorption properties. By forming an unsynchronized structure, large-bandgap GQDs can be used for highly selective UV detection. In lithium or sodium ion batteries, GQDs can aid in reducing volume expansion, promoting electron transfer and lithium/sodium diffusion, enhancing electrochemical properties, and strengthening the double-layer surface.[37]

GQDs, due to their quantum confinement feature, have a size-dependent band structure. Additionally, their two-dimensional surface exhibits strong non-covalent interactions with biological molecules through π–π interactions and hydrogen bonding, providing a chemically tunable platform for bio-conjugation. Therefore, they have found extensive applications in fluorescent sensors as tunable fluorophores and fluorescence quenchers, laying the foundation for expanding fluorescent sensors and biological imaging systems.[38] Using fluorescent GQDs presents a chance to enhance the efficiency of fuel cells, biological imaging, and light-emitting gadgets. These are employed as fluorescent agents to detect mineral ions, large biomolecules, and small molecules with high sensitivity.[5] Due to their small PL size, GQDs are highly sensitive to environmental disturbances and can interact with small molecules.[5,37] Optical sensors based on GQDs have been used for detecting food poisoning, insecticides, and heavy metal ions. With their good light absorption properties, excellent light stability, fully accessible surface, and tunable band gaps, GQDs have been used as photocatalysts for pollutant degradation, H_2 evolution, and CO_2 reduction.[37]

GQDs have an infinite Bohr radius, demonstrating the effects of quantum confinement with random sizes. They exhibit PL with a non-zero bandgap on excitation, leading to the alignment of HUMO and LUMO bands in the spectrum from UV to infrared (IR). Therefore, these properties can be adjusted by changing their shape, edge configuration, surface chemistry, size, and chemical doping. The band gap can be modified to cover a wide range of solar radiation.[39]

On a larger scale, GQDs and GQD-based nanocomposites can be implemented in wastewater treatment plants (WWTPs). As it stands, most currently available WWTPs were primarily designed to target the removal of only biodegradable compounds and not emerging complex compounds.[11]

Mining wastewater is rich in heavy metals that are known to be toxic to aquatic life and humankind, while hospitals and pharmaceuticals could release wastewater loaded with drugs such as antibiotics, resulting in the development of drug-resistant bacteria.[40–42] Antibiotics belong to a class of pollutants known as 'pollutants of everyday concern', which have captured global interest because their fate in the environment is not yet fully understood. Despite the diversity and complexity of wastewater matrices, the treatment regimes are standard and have stayed the same over the years. Consequently, some of the emerging pollutants are able to sneak past the treatment train and end up in our tap water, where they could cause various adverse health effects.[43–46] Therefore, a need exists to modify, improve, or even couple current wastewater treatment processes with advanced techniques that will enable the removal of emerging pollutants from wastewater before being discharged into receiving dams.[47]

Research on advanced carbonaceous nanomaterials such as GQDs has been on an exponential trajectory as potential materials for environmental applications because of their unusual and exotic properties. The objective of this research is to examine the characteristics of GQDs, which render them appropriate for the purification of wastewater,[43] especially for organic pollutants.[48] The raw materials used in the fabrication of GQDs, the methods to fabricate GQDs, and their characterization will be discussed in this review paper.

Primary materials used for the production of GQDs

Recently, several primary materials have been used to derive GQDs, including carbon sources such as animal manure,[49] humic acid,[50] dried pine needles,[51] rice husk,[52] cow milk,[53] honey,[54] corn powder,[55] bean leaves,[56] bamboo wood,[57] ammonium citrate,[58] *Bougainvillea spectabilis* flower petals,[59] grapefruit extract,[60] graphite micro-particles,[61] maltose[62] and citric acid.[63–65] Natural sources such as graphite have also been used as a precursor for preparing GQDs recently, as graphite does

not have enough functional groups, and the yield of GQDs from graphite is not high. Methods to increase the yield of GQDs from graphite have been investigated.[66] Recent studies have focused on developing simple and low-complexity approaches to convert waste into graphene nanomaterials.[67] Studies have documented the synthesis of GQDs from biomass, viewing biomass as a discarded resource that can be utilized to generate a nanoscale product.[68,69] In most GQD syntheses, citric acid has been used as a precursor because it is a common organic acid that contains active groups, including –OH and C=O groups. Citric acid is undoubtedly the most popular carbon precursor because it is inexpensive, biocompatible, and easy to supply. The materials obtained from it also have high PL and quantum yield (QY).[49] Instead of using raw citric acid, other sustainable carbon sources can be used, same as grass clippings,[66] coffee grounds,[70] and tea waste.[71] However, renewable raw materials such as biomass comprise products with different weights, such as amino acids, sugars, biopolymers, hydroxy, or other raw materials found in natural resources. Biomass and its components, such as organic acids and carbohydrates, are the only renewable carbon sources and vital precursors to carbon materials. It is well known that carbon-based materials possess the most effective properties among all resources on the Earth, such as easy conductivity, high porosity, resistance to acid and alkali, and lightweight.[49]

GQDs have been reported for the synthesis of PL on a large scale and at a low cost based on the carbonization of multi-ring aromatic hydrocarbon precursors.[72] Glucose has been utilized as a raw substance for obtaining GQDs in many studies.[73,74] In addition, lignin has been used as a primary material for making GQDs because it has significant advantages that are environmentally friendly. Lignin is rich in carbon-containing *p*-hydroxyphenyl units, guaiacyl units, and syringyl units, which are of great importance. Nair *et al.* investigated lignosulfonates as a carbon source for preparing of GQDs to detect toxic metal ions in water.[75] Lignin is the second most abundant organic element in the world of vegetation; however, removing and converting lignin into products is a critical point and an issue for valuing dedicated or residual biomass as renewable fuels and chemicals.[76] Agricultural wastes, such as oil palm fibers, coconut husks, date stones, *etc.* are considered active carbon sources.[77] The empty fruit bunches of oil palm (OPEFB) are one of the main wastes in the oil industry and are used as a renewable energy source. In Malaysia and Indonesia, more than 15 and 7 million tons of OPEFB are produced annually, respectively.[78] Due to the expansion of palm oil production in Malaysia, a large number of empty fruit bunches (EFBs) are produced, which is harmful to the environment. EFB contains abundant carbon and lignin, making it a good precursor for producing activated carbon, which is a suitable adsorbent for various industries such as wastewater treatment and organic pollutant removal.[77]

Methods used in previous studies to fabricate GQDs

The electrochemical oxidation process involves the electrochemical cleavage of carbon precursors into GQDs, typically under high redox voltage. Electrochemical oxidation can occur in one of two ways; the first is where C–C bonds of the carbon material are cleaved *via* chemical oxidation, and the second occurs when either the oxygen free radical ($O^{\bullet}$) or the hydroxyl free radical ($^{\bullet}OH$) from water attacks and cleaves the C–C bonds to form GQDs. The advantages of using this method include the formation of stable GQDs and production of high-quality GQDs.[11] Dong *et al.* oxidized SWCNTs with 8 M HNO_3 and then heated the oxidized SWCNTs in water at a temperature of 200 °C, which led to the disintegration of SWCNTs and the accumulation of graphene nanosheets. Two types of GQDs with various optical attributes were obtained.[5] GQDs with sizes ranging from 5–3 nm and a thickness of 0.93 nm have been synthesized by electrochemical oxidation of graphene for single-layer graphene as reported by Luo *et al.*[79] Li *et al.* offered an electrochemical route for preparing water-soluble GQDs using a graphene film as the working electrode.[80] Shin *et al.* used mild oxidation for layering from several sources of MWCNTs, CF, and charcoal, resulting in blue fluorescent GQDs.[81]

MCNTs or graphite containing sp^2-hybridized carbon is used in electrochemical exfoliation, which is a two-step process. Initially, an oxidation potential is applied to the layered bulk material immersed in an electrolyte. As a result, sp^2 bonds are cleaved, and solvent molecules or electrolytes intercalate between the layers of the bulk material. The resulting product is then electrochemically reduced by applying an appropriate cathodic potential. The precise control of the applied potential enables highly selective oxidation in layered bulk materials, unlike solvo-/hydro-thermal techniques, where oxidation remains uncontrolled.[82] Based on a prior study, the preparation of GQDs has been reported by electrochemical exfoliation using a graphite electrode through the reaction between the oxidation of the anode and the intercalation of anions in an ionic liquid. Electrochemical fabrication of GQDs with smooth edges and fewer defects in uniform sizes of 3, 5, and 8.2 (±0.3) nm from MWCNTs has been reported, where the PL attributes of GQDs can be tuned by changing the diameter of CNTs, supporting electrolyte concentration, electric field, and temperature.[83] Bahadori *et al.* prepared GQDs by thermal treatment of two graphite rods before chemical oxidation in an electrolyte containing NaOH and citric acid instead of graphite rods and electrolysis. The thermal treatment at a temperature of 1050 °C created surface defects on graphite rods that created more active sites to facilitate electrochemical reactions.[81]

In addition, ultrasound technology is a common method for synthesizing materials.[84] For example, GQDs produced by ultrasound waves can create high-pressure and alternating low waves in the liquid, and the resulting mechanical force can break carbon–carbon bonds to cut GQDs.[85] The synthesis of GQDs necessitates using glucose precursors, carbon sources and polymerization in the same manner as mentioned above, which can help in controlling GQD size by increasing the reaction rate and reducing-edge defects in graphite layers.[79] In another strategy, the synthesis of bright GQDs with high quantum yields and short reaction times using only GO and $KMnO_4$ has been reported using ultrasound in a one-step synthesis.[86]

In a study, Nike *et al.* presented a one-step synthesis of GQD using thermal citric acid decomposition.[87] The procedure of preparing GQDs using thermal acid citric acid decomposition involves heating and melting of 5 grams of citric acid, resulting in transformation to a dark orange color in 25–30 minutes. Then, a 1.5 M solution of NaOH was added dropwise in a concentrated solution of melted citric acid at room temperature. After adding sodium hydroxide, GQDs with pH values ranging from 8 to 12 will be obtained. Therefore, pH plays an important role in forming GQDs from citric acid (Fig. 2).[88] Wang and colleagues prepared highly fluorescent nitrogen-doped graphene quantum dots (N-GQD) using ammonium citrate as a carbon starting material through direct carbonization.[5,81]

Additionally, the synthesis of GQDs using trisodium citrate through a pyrolytic carbonization pathway and two-step purification by ultrafiltration has been reported.[89] Furthermore, dual-precursor approaches were employed in the pyrolysis method for GQD preparation. Liu and colleagues prepared GQDs with multicolor PL and uniform size using hexaphenylhexa-*peri*-hexabenzocoronene as a substitute for carbon, which exhibited a high PL efficiency of over 3.8%.[90] Tang and colleagues proposed a combination of hydrothermal and microwave methods for faster pyrolysis of glucose.[80] Recently, Li and colleagues used a D-glucose precursor to prepare single-crystalline GQDs, which had a hexagonal crystal structure with dimensions of 5 nanometers and exhibited blue fluorescence.[81]

Another method for preparing GQDs is the pulsed laser ablation (PLA) technique. PLA can be used for carbon-based raw materials precipitating in organic or aqueous solvents, producing particles with modified surfaces.[84] PLA is a simple and clean process.[91] The PLA method offers advantages such as one step synthesis, shorter synthesis time, good reproducibility, and minimal experimental setup.[92] However, several articles have reported the preparation of GQDs through the PLA method. The Kolmogorov explosion model was used to describe the carbon material erosion mechanism by PLAL.[11] Thongpool and colleagues synthesized GQDs from graphite targets using the PLA method[91]. Shen's group synthesized several PL-adjustable GQDs by controlling the PLA time, which showed a change in color dispersion from green to blue using MWCNTs as carboxylic acid agents.[92] In a study focused on preparing GQDs from graphite pieces using high-power ultrasound-assisted PLA, 500 mg of graphite pieces were scattered in 200 mL of ethanol using high-power ultrasound waves during the laser ablation process. When this high-power ultrasound was not applied, the accumulation of graphite pieces led to plasma column formation.[91]

GQDs have been synthesized using microwave-assisted techniques, which have evolved to overcome time-consuming reaction limitations associated with methods such as hydrothermal methods.[11] The microwave method enables a faster synthesis of GQDs.[79] Microwave heating can compensate for deficiencies.[93] This approach has several benefits, such as production of large quantities of products, high consistency, ease of handling, and energy conservation.[93] Additionally, this method does not require an activating agent as the size of the GQDs increases with longer heating times.[79]

Zhang *et al.* synthesized water-soluble GQDs, as shown in Fig. 3, by reacting water with aspartic acid and NH_4HCO_3 and heating (10 minutes) using a 560 watt microwave reactor. The successfully synthesized GQDs have lower cellular toxicity and high optical stability.[94] Researchers examined the effect of the citric acid additive under microwave heating. Mono-hydrated citric acid (0.80 g) was weighed and ground into a fine powder in a deep mortar, and then irradiated for 4 minutes in a 700 watt household

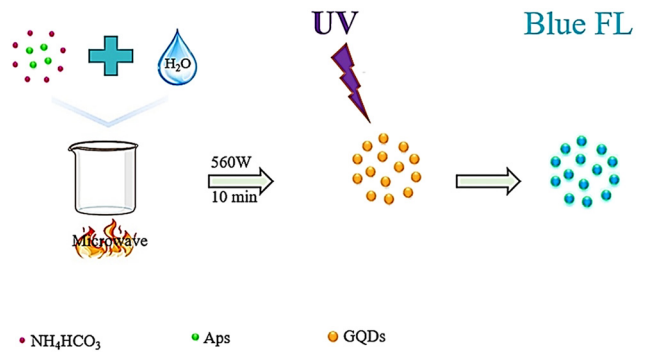

Fig. 3 Schematic representation of the water-soluble GQD fabrication process. Reproduced with permission from ref. 94. Copyright (2016) Elsevier.

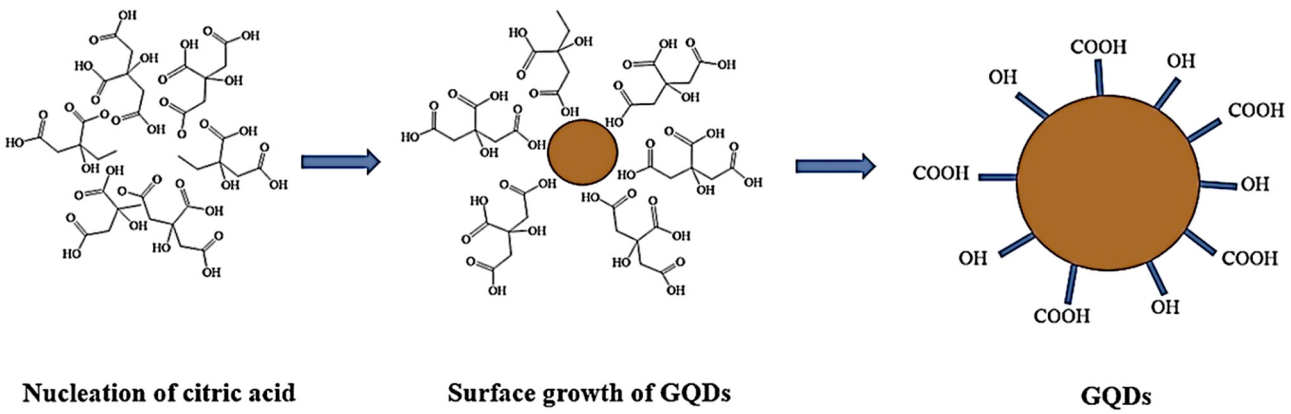

Fig. 2 Preparation of GQDs, using citric acid as a precursor. Reproduced with permission from ref. 88. Copyright (2017) Springer Nature.

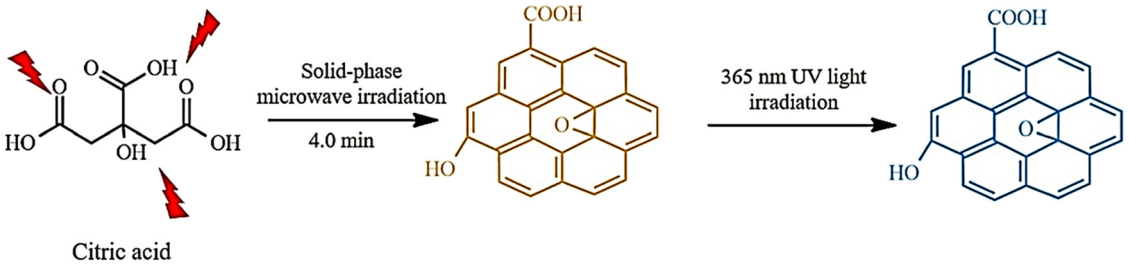

Fig. 4 Microwave-assisted, solid-phase fabrication of GQDs. Reproduced with permission from ref. 93. Copyright (2016) Wiley.

microwave. After cooling, the dark coffee-colored compound was dissolved in a 1 mol L^{-1} NaOH solution and dialyzed for three days. The prepared GQDs showed excellent light stability, PL properties, ion power, low cellular toxicity, and good solubility. GQDs prepared from dry food additive citric acid using the action of microwave irradiation are probably harmless to the human body. The mechanism of GQD formation is exhibited in Fig. 4.[93]

The research was conducted on a microwave-based eco-friendly method for producing bright red GQDs by utilizing ethanol extracts derived from the leaves of *Mangifera indica* (mango).[56,79] Mango leaves were found to be a good precursor for preparing GQDs. The mixture was heated in a microwave oven at 900 watts for 5 minutes, and the remaining solution was dispersed in absolute ethanol for suitable m-GQD dispersion.[56] Additionally, GQDs synthesized from cow milk using one-step microwave heating were reported.[53]

In previous studies, simple hydrothermal and solvothermal approaches have been used for synthesizing GQDs, which are almost similar except that water is used as a solvent in hydrothermal synthesis while dimethylformamide is used as a solvent for the solvothermal method.[79] The thermal and hydrothermal methods involve various techniques of crystallizing materials from high-temperature aqueous solutions to high vapor pressures. The fabrication of single-crystalline GQDs through the hydrothermal method has been demonstrated by many researchers.[95]

During the preparation process, carbon-based materials undergo exposure to powerful oxidants and are subsequently transformed into GQDs through high temperature and pressure cutting. This process involves oxidizing carbon materials with potent oxidants, which introduces oxygenated functionalities into the carbon network. Subsequent oxidation then takes place at ambient temperatures. Under hydrothermal conditions, oxygen from epoxy bonds and unstable carbonyl pairs form GQDs. In hydrothermal and solvothermal synthesis approaches, temperature plays a vital role in the structure of GQDs. At higher temperatures, small and highly crystalline GQDs are produced. In contrast, unsuitable GQDs are synthesized at lower temperatures.[11]

Zho *et al.*[96] investigated the synthesis of GQDs using a solvent, thermal method using GO sheets, and DMF solvent.[79] Pan *et al.* synthesized bright blue GQDs. The GO sheets were oxidized before thermal treatment. The oxidation stages include carbonyl groups, carboxylic acid functional groups, and epoxy groups, which act as a breaking point under hydrothermal conditions, resulting in the production of fully broken GQDs.[81] GQDs have been synthesized using a one-step hydrothermal procedure with high efficiency. The materials used as primary sources were maltose, citric acid, and deionized water.[62]

GQDs were produced from bamboo timber waste (Bf) using a one-step hydrothermal technique. Initially, Bf-CNCs (200 mg) were dispersed in deionized water (200 mL) and sonicated for 20 minutes. The resulting mixture was then placed in an autoclave and kept at 180 °C for 8 hours. Upon completion, the materials were cooled and subjected to ultrasound for 10 minutes. The dark brown product was then filtered using a membrane to remove insoluble carbonaceous materials and kept for 24 to 36 hours before being washed through a dialysis bag.[57]

In another study, highly fluorescent GQDs were successfully synthesized using a humic acid precursor derived from lignite. The process involved hydrothermal treatment of humic acid in a basic solution using an autoclave at 200 °C for 12 hours. Finally, to remove large particles, the solution was centrifuged for 20 minutes. The resulting liquid was dialyzed for 48 hours against water to obtain pure GQDs. This precursor significantly reduced production costs.[50]

Furthermore, another report discusses the preparation of fluorescent GQDs from coffee grounds as a raw material, without the need of strong acids or extended catalysts. In summary, coffee grounds were separated from ground beans and cleaned with deionized water before being dried and subjected to hydrothermal treatment at a temperature of 200 °C. The resulting GQDs were treated with PEI under hydrothermal conditions at a lower temperature (120 °C) to prevent PEI from undergoing molecular changes.[70] Table 1 introduces a list of raw materials, fabrication methods, and application of GQD, reported in previous studies.

Methods and analysis used to describe GQDs

Various methods are utilized to comprehend the structures, morphology, and composition of particles based on their size and shape, regardless of their intended use. Despite having unique optical and physical characteristics, the properties of GQDs must be identified and linked to different measurement techniques. These techniques include Raman, UV-vis, X-ray diffraction (XRD), atomic force microscopy (AFM), PL transmission microscopy, X-ray photoelectron spectroscopy (XPS), and infrared (FTIR) for analyzing fluorescence properties, electronic states, crystal structures, surface morphology and vibrational patterns and functional group composition. The choice of

Table 1 Raw materials and methods used for the synthesis of GQDs and the application of the products

Raw materials	Methods	Size (nm)	Yield (%)	Applications	Ref.
Corn straw	Hydrothermal	—	—	Detection of PO_4^{3-}	97
Leaves of curry tree	Hydrothermal	2.49 ± 0.03	14.4	Detection of AFB_1	98
Cellulose	Hydrothermal	1–5(>5)	19.4	Bioimaging and biolabeling	99
Coffee grounds	Hydrothermal	1.88 ± 0.72 and 2.67 ± 0.81	—	Imaging and measurement of heavy metals	70
GO	Hydrothermal	5–19	7.4	Bioimaging	100
Tea waste	Hydrothermal	5–20	84	Detection Fe^{3+}	71
Rice husk	Hydrothermal	0.2503 ± 0.006	—	Extraction of La(III) from water	101
Orange peel waste	Hydrothermal	—	—	Detection of Fe^{3+}	102
1,3,6-Trinitropyrene	Hydrothermal	2.5	—	Detection of Ag^+	103
GO	Hydrothermal	4.3 ± 0.8	—	Photovoltaic, biological and light emitting devices	104
Maltose, hydrochloric acid	Hydrothermal	1–3	—	Photodegradation of imipramine	62
Dhruva grass	Solvothermal	3–5	49.1	PL property	105
Citric acid	Solvothermal	—	—	H_2S gas detection	106
Aspartic acid and NH_4HCO_3	Microwave	1–5	12	Cellular imaging	84
Mango leaf	Microwave	2–8	—	*In vivo* biological imaging	56
Citric acid	Microwave	7.5 ± 2.3	3.2	Cellular imaging	93
Citric acid	Microwave	5–10	—	The detection of iron ions and paraquat	107
Cow milk	Microwave	~5	—	Bioimaging and drug delivery	53
Grape seed	Microwave	1–8	53.6	Application of measurement	60
MWCNTs	PLA	1–5	12	Photoelectric	84
MWCNTs	Electrochemical exfoliation	3, 5, 8.2(± 0.3)	5.1–6.3	Cellular and molecular imaging	83
Graphite rods	Electrochemical exfoliation	~3.5–7.3	—	Biological imaging	108
Citric acid	Pyrolysis	1–4	62.8	Cellular imaging	109
Trisodium citrate	Pyrolysis	1.3 ± 0.5	3.6	Biological imaging	89
Honey	Pyrolysis	2.4	3.6	White-light emitting	54
Citric acid	Pyrolysis	2–3	3.8	*In vitro*/*in vivo* imaging	90

specific characterization technique depends on the type of GQDs being studied.[7]

Fourier transform infrared spectroscopy (FTIR)

FTIR is a crucial method for identifying surface components and functional groups on materials qualitatively. As IR radiation passes through a sample, some of it is absorbed by molecular vibrations while the rest is transmitted. The molecular vibration state produces a distinctive signal for each molecule in the fingerprint region, which researchers use to examine functional groups on the surface of GQDs.[7] As shown in Fig. 5, FTIR results were obtained to confirm the interaction between functional groups and materials in GQDs. The GQD result is indicated by some vibrational peaks that are related to others. The notable band is located at 1585 cm^{-1} corresponding to the stretching mode of C=C. Next, the peaks are related to O–H (3400 cm^{-1}), C–H peaks (2976 and 1376 cm^{-1}), and C–O (1206 cm^{-1}).[62]

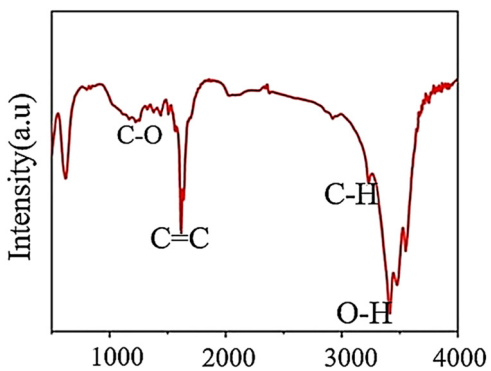

Fig. 5 FTIR pattern of GQDs. Reprinted with permission from ref. 62. Copyright (2020) Springer Nature.

High-resolution transmission electron microscopy (HRTEM):

HRTEM provides the possibility of visualizing GQDs and information about the distribution, shape of particles, crystallinity, and edge types. The result obtained from HRTEM can be confirmed with XRD data.[11] Fig. 6a shows the TEM images of dispersed GQDs in water. In the TEM image, the diameter of GQDs mainly lies in the range of 1.8–2.4 nm with an average size of 2.1 nm. As shown in Fig. 6b, HRTEM images show high crystallinity of GQDs with lattice parameters of 0.25 and 0.33 nm, respectively, considering that the interplanar distance of graphite is 0.335 nm.[94]

UV-vis spectroscopy

UV-vis is a type of absorption spectroscopy that examines the electronic transitions of materials in UV and visible regions and occasionally in the near-infrared range. The electromagnetic spectrum is generated when the atoms or molecules undergo electronic transitions from ground to an excited state after absorbing in the UV region. The relationship between the energy absorbed and an electronic transition in terms of wavelength (λ) or frequency (ν) for a transition is given below:

$$\Delta E = h\nu = hc/\lambda$$

where h = Planck's constant and ΔE = energy absorbed during electronic transition in a molecule from the ground state to the excited state. The Lambert–Beer law is an important and more

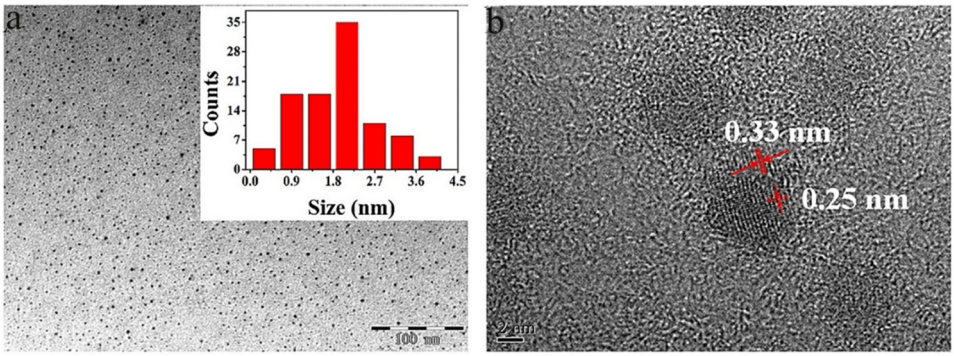

Fig. 6 Typical TEM image (a) and HRTEM image of GQD (b). Reprinted with permission from ref. 94. Copyright (2016) Elsevier.

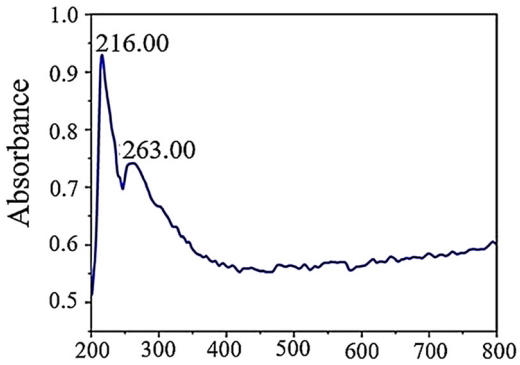

Fig. 7 UV-vis absorption spectra of GQDs. Reprinted with permission from ref. 62. Copyright (2020) Springer Nature.

convenient expression for UV absorption, which relates absorption (A) directly to the concentration (c) of the absorbing species.

$$A = \epsilon cl$$

where ϵ is the molar extinction co-efficient, and l is the cell-path length.[7]

In an aqueous solution, GQDs exhibit absorption peaks at 263 and 216 nm in their UV-vis absorption spectrum. These peaks are associated with π–π* electronic transitions from C═O and π–π* transitions from C═C. The peak observed at 263 nm is attributed to electron transfer from π–π* due to electronic transitions involving sp^2 carbon structures from C═O. On the other hand, the peak at 216 nm corresponds to π–π* transitions involving C═C bonds since these transitions occur within the wavelength range of 200–270 nm in GQDs. Fig. 7 provides a visual representation of this phenomenon.[62]

Fluorescence spectroscopy analyses

Fluorescence spectroscopy analyzes fluorescence or PL from a specimen. It is a complementary phenomenon to UV–vis spectroscopy, where a beam of UV light excites the electrons in molecules of certain compounds, leading to emission of light. It is primarily associated with the electronic, and vibrational states and the sample preparation involves the use of a solution using the desired solvent. PL spectrum measurement for GQDs is essential due to their strong fluorescence properties. For a typical measurement, the GQDs sample is excited with specific excitation wavelength, and the GQDs emit corresponding emission peaks. The literature reveals that GQDs show either excitation-dependent or -independent emission in different color regions or emission light such as blue, green, yellow, cyan, and red luminescence.[7] In investigating the optical characteristics of manufactured GQDs, PL experiments were conducted using diverse excitation wavelengths. As demonstrated in Fig. 8a, when the excitation wavelengths enhanced (300 to 420 nm), the intensity of the emission peak at 320 nm rose to a peak and then decreased. The PL spectrum

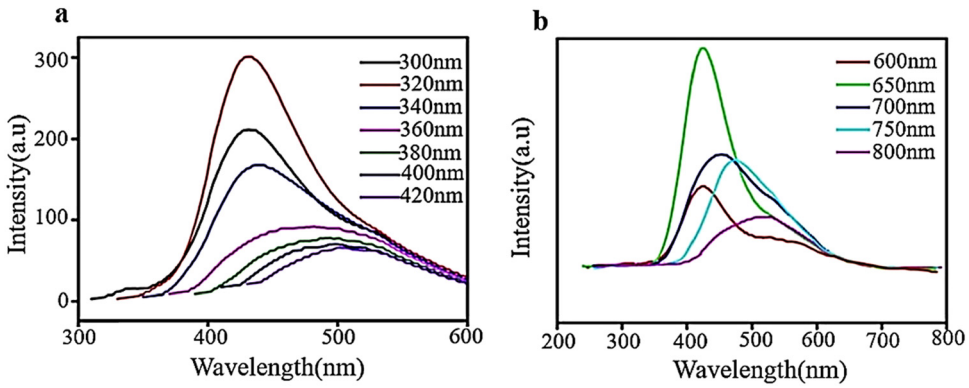

Fig. 8 PL spectra of aqueous solution of GQDs at diverse excitation wavelengths ((a) and (b)). Reprinted with permission from ref. 110. Copyright (2016) Elsevier.

exhibits the strongest emission peak centered at 430 nm with no evident shift under excitation wavelengths from 300 to 340 nm. However, when the excitation wavelength is altered (340–420 nm), the PL peaks move toward longer wavelengths with wider bands, and the most intense peaks are observed around 500 nm. The observed photoluminescence red-shift of GQDs was accompanied by a significant reduction in photoluminescence intensity, which is a signature of the gradual evolution of the confinement in quantum dots.[110] The PL behavior depends on the particle sizes that can be excited by a particular wavelength. Smaller particles will exhibit the PL effect at shorter wavelengths, while larger particles will exhibit the PL effect longer wavelengths.[111]

As shown in Fig. 8b, the intensity of GQD emission peaks increased without any shift when excited from 600 to 650 nm and then decreased with a change in color from red when excited from 650–800 nm. The spectra exhibit the most intense emission peaks at approximately 420 nm when excited with a wavelength of 650 nm and a shift towards the red end of the spectrum when excited with longer wavelengths. These results demonstrate that PL is dependent on excitation and shows how PL characteristics are transformed at an excitation wavelength of 600–800 nm. The excitation-dependent emission properties of GQDs may be related to their highly defective structures with a great number of sp^3 and vacancy defect states in the basal plane.[110]

Raman spectroscopy

Raman spectroscopy is a crucial technique that provides insights into molecular vibrations and is extensively employed for examining materials, particularly nanomaterials based on graphene. It can uncover details about the electronic structure, crystal structure, and lattice vibrations of materials. Raman bands arise due to alterations in polarizability and are helpful for investigating the electronic structure and surface defects of carbon-based substances such as GQDs and nanotubes, where the defect (D band) and tangential (G band) modes exhibit systematic variations.[7] The Raman spectrum of GQDs in Fig. 9 shows the D and G bands observable in the sample. The G peak at 1574 cm^{-1} determines good crystallinity of GQDs and relates to sp^2 vibration on the carbon plane. The D peak at 1381 cm^{-1} is associated with defect states in GQDs due to multiple edge effects, corresponding well with hydrothermal methods that create highly functional surface defect groups.[62]

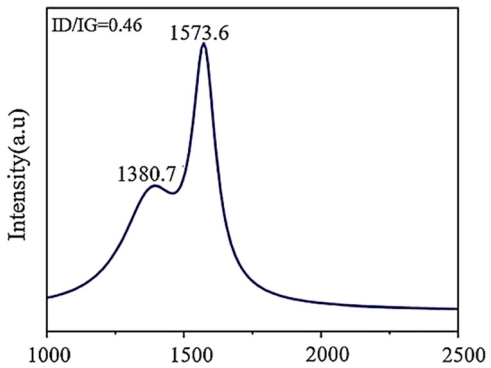

Fig. 9 Raman spectra of GQDs. Reprinted with permission from ref. 62. Copyright (2020) Springer Nature.

Atomic force microscopy (AFM)

AFM is a versatile and powerful microscopic technique which gives insights into the surface topography of the sample. It uses a cantilever with a very sharp tip to scan across a sample surface and operates either in a contact or non-contact mode. The cantilever is brought significantly closer to the surface; increasingly, repulsive force takes over and causes the cantilever to deflect away from the surface, helping us to learn about the topography of the solid surface through the tip scanning the surface. It is usually used to investigate the thickness of GQDs and further estimate the number of graphene layers.[112]

X-ray diffraction

XRD is a crucial technique for determining the amorphous phase or crystalline phase and assessing the level of crystallinity, and the particle size distribution of various nanomaterials. It is particularly significant in obtaining valuable information about the dimensions of the unit cells by accurately identifying the atoms' arrangement.[7] The XRD pattern of the synthesized GQD reveals a broad peak located at $2\theta = 25^\circ$ (Fig. 10), which suggests that the material is composed of an irregular arrangement and disorganization due to oxygen molecules with functional groups.[113]

X-ray photoelectron spectroscopy (XPS)

XPS is a quantitative technique that is useful for analyzing the surface (0–10 nm surface depth) elemental chemistry of a sample and is based on the well-known photoelectric effect first. The elemental composition, and oxidation state of the element present at the surface of the sample could be extracted from XPS analysis. It is always used along with FT-IR to study the material surface components, the functional groups. A low-energy X-ray is irradiated on the sample surface to excite the electrons of the sample atoms, and a photoelectron is generated if their binding energy is lower than the X-ray energy. By measuring kinetic energy, the binding energy could be derived, and the corresponding characteristic peaks could be obtained. The overall process is given below:[112]

$$A + h\nu = A^+ + e$$

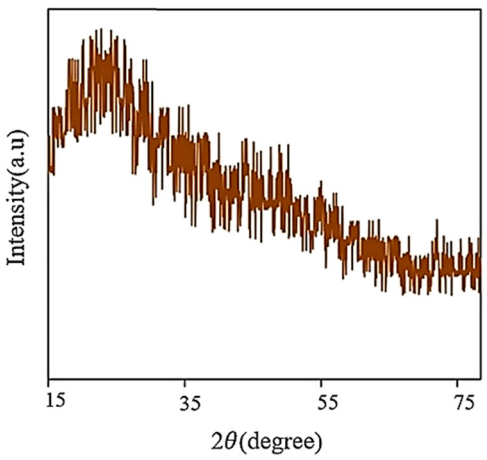

Fig. 10 XRD pattern of GQDs. Reprinted with permission from ref. 113. Copyright (2020) Elsevier.

where A = surface of the species, A^+ is the oxidation state of the surface species, and $h\nu$ is the energy of photon; then, according to the conservation of energy

$$E(A) + h\nu = E(A^+) + E(e)$$

where $E(A)$ and $E(A^+)$ are the respective energy of the species A and A^+ and $E(e)$ represents energy of the electron; since, the electronic energy is kinetic, we get

$$\mathrm{KE} = h\nu - (E(A^+) - E(A))$$

$$\mathrm{KE} = h\nu - \mathrm{BE};$$

where KE = kinetic energy and BE = binding energy

The BE of solids is conventionally measured with respect to the Fermi level of the solid instead of the vacuum. It involves a small correction term called the work function (φ) of the solid,

$$\mathrm{KE} = h\nu - \mathrm{BE} - \varphi$$

There are several studies investigating the elemental composition and doping of GQDs by XPS spectroscopy.[69,114,115]

Performance and application of GQDs

Use of GQDs as photocatalysts. GQDs are more desirable as photocatalysts compared to other types of carbon materials because they have basal planes that allow for enhanced contaminant adsorption. Furthermore, GQDs can function as electron donors or acceptors, which helps regulate the charge produced by light and enhance the photocatalytic activity of GQD nanocomposites. This improved efficiency is relevant to the capacity of GQDs to assist in absorbing organic pollutants.[11] Table 2 summarizes the usage of GQDs in environmental remediation.

Liu *et al.* created a combination of GQDs and modified mesoporous graphitic carbon nitride (mpg-C_3N_4) through electrostatic interaction, which was used to degrade RhB through photodegradation. The effectiveness of the photocatalytic process was determined by measuring the removal of RhB. The composite with 0.5 wt% GQDs/mpg-C_3N_4 showed the highest efficiency, with a 97% removal rate under visible light. The improved photocatalytic activity was due to the incorporation of GQDs as electron acceptors.[130] In another study, ZnS nanowires decorated with GQDs were investigated by a simple hydrothermal method. ZnS nanowires were decorated with GQDs through a self-contact process *via* electrostatic adsorption onto the surface of ZnS nanowires and a subsequent intense bonding process through thermal reduction of GQDs onto ZnS nanowires. The bandgap energy of the GQD/ZnS nanocomposite was lower than that of pristine ZnS nanowires. The as-prepared photocatalysts, due to their effective separation of photo-induced electron–hole pairs, showed an enhanced photodegradation efficiency towards RhB compared to individual components (Fig. 11).[33] It was found that decorated GQDs introduced additional visible light response and acted as influential electron collectors and transfer agents to efficiently suppress electron–hole recombination, thus significantly enhancing the photocatalytic properties of ZnS nanowires. The photocatalytic rate constant for GQD/ZnS nanocomposites in RhB photodegradation reaction was 14 times higher than that of commercial ZnS.[33,131]

In recent research, the use of GQDs in environmental photocatalysis has been investigated. The study revealed that the efficiency of TiO_2 photocatalysis was enhanced by incorporating GQDs, resulting in better degradation of MB.[11] A low-cost wet chemical method was used to create GQDs of varying sizes, using birds' nest charcoal as a starting material. These GQDs have PL and visible light absorption properties and are typically combined with TiO_2 to form TiO_2–GQD nanocomposites. The bandgap of GQD nanostructures can be adjusted, potentially increasing light absorption in TiO_2. The combination of these materials reduces carrier recombination, increases carrier mobility, and improves overall conversion efficiency. Compared to pure TiO_2, the composites showed higher photocatalytic properties and rate constants. The photocatalytic activity was evaluated using the MB photodegradation experiment, with results (Fig. 12) indicating that coupling GQDs with TiO_2 enhances visible light absorption and limits non-recombination reactions of carriers. The 1 wt% GQD–TiO_2 composite exhibits the highest rate constant compared to other TiO_2–GQD composites.[132]

The study employed a one-step hydrothermal technique to obtain a concentrated yellow solution of GQDs and TiO_2 NTs. The TiO_2 NTs/GQDs composite was produced by immersing TiO_2 NTs in the GQD solution through hydrothermal immersion. Fig. 13 depicts the potential mechanism for enhancing photocatalytic activity in the composites, which can be explained by three characteristics. Initially, coupling TiO_2 NTs with GQDs increases the visible light absorption of TiO_2 due to electronic coupling between the π states of essential graphite GQDs and the conduction band states of TiO_2. Afterward, GQDs act as an electronic reservoir to capture photo-generated electrons from TiO_2NTs and enhance the electron–hole pair separation, as authenticated by PL measurements. Additionally, up-conversion GQDs effectively transfer long-wavelength radiation to short-wavelength radiation used by TiO_2 NTs/GQDs composites. Oxygen absorbed on the surface of GQDs accepts electrons to form O^{2-} and directly oxidizes MO on the oxide surface. Simultaneously, holes on the H_2O/OH surface oxidize TiO_2 more, producing OH• radicals that help degrade MO into H_2O and CO_2. Furthermore, a 2.5% weight ratio of TiO_2NTs/GQDs exhibited the best degradation.[110]

GQD nanocomposites as adsorbents for heavy metal removal

A study was carried out to develop new hydrogel beads that possess magnetic and bioabsorbent properties. These beads were created using chitosan gum, polyvinyl alcohol, and GO through the gelation method in a boron acetone solution. The beads were thoroughly analyzed and found effective in removing heavy metal ions such as Pb(II) and Cu(II) from water solutions. The efficiency of ion removal is dependent on the charges of the magnetic beads. The rate of adsorption was explained using a pseudo-second-order kinetic model, and the experimental data were well-suited to the Langmuir isotherm with maximum adsorption capacities of 69.97 and 81.78 mg g^{-1} for Cu(II) and Pb(II), respectively.[134]

Table 2 Diverse starting materials and synthesis methods for GQD-derived nanocomposite fabrication and their applications in environmental remediation

Nanocomposite	Precursor	Synthesis method	Application	Highlights	Ref.
GQD/TiO_2	Graphite	Hydrothermal	Photodegradation of MB	By adding just 2% of GQDs to TiO_2 nanotubes, the band gap of the resulting composites can be adjusted, allowing for the degradation of 96.7% of dye in just 120 minutes when exposed to visible light	116
N-GQD/TiO_2	Citric acid	Hydrothermal	Photodegradation of MB	Photodegradation efficiency of TiO_2 toward MB using UV is enhanced from 40 to 85%: Nanocomposite degraded 85% of the MB (70 min)	117
GQD/TiO_2	Citric acid	Pyrolysis	Photodegradation of RhB	GQD/TiO_2 degraded 100% of the RhB (half-hour)	118
GQD/TiO_2 NTs	Graphite	Hydrothermal	Photodegradation of MB	The 2.5 wt% NTs/TiO_2/GQDs depicted the highest degradability, which is about 2.7 times higher than pure TiO_2NTs	110
GQD/ZnS	Carbon fibers	Hydrothermal	Photodegradation of RhB	Nanocomposite degraded 90% of the RhB within 40 min	33
GQD-PVP-CdS	Citric acid	Hydrothermal	Photodegradation of MO	With 92.3% of MO removed after 3 hours of visible light illumination	119
Bi_2S_3-GQD/TiO_2	Citric acid	Pyrolysis	Removal of Cr^{6+} and MO	Rate of dye degradation: under irradiation 52–92%	120,121
Ag/N-GQDs/g-C_3N_4	Citric acid	Pyrolysis	Tetracycline removal (TC)	The best combination of Ag/N-GQDs/g-C_3N_4, containing 0.5% N-GQDs and AgNPs, exhibits a removal rate of 93, 90 and 31% for TC when exposed to light with wavelengths greater than 365, 420, and 760 nm respectively	122
GQD/ZnO	Citric acid	Pyrolysis	Degradation of metronidazole	Highly optimized GQD/ZnO composite depicted ultra-high-rate constant (~1.74 times higher than the pristine ZnO)	123
N-GQD/$BiVO_4$	Citric acid	Hydrothermal	MB degradation	Almost 90% of MB was degraded by 5 wt% N-GQD/$BiVO_4$ after 200 min irradiation	124
TiO_2/Sb_2S_3/GQDs	Corn powder	Solvothermal	Investigating anti-microbial attributes towards *S. aureus* and *E. coli*	The combination of TiO_2, Sb_2S_3, and GQD in the nanocomposite resulted in a significant decrease in the minimum inhibitory concentration (MIC) for *S. aureus*, and *E. coli* with values of 0.1 and 0.03, respectively	125
$CoFe_2O_4$@HAP-GQDs	Citric acid	Solvothermal	Removal of brilliant cresyl blue dye (BCB)	Maximum BCB removal rate (R%) reached 93	126
Fe_2O_3-GQD/NF-TiO_2	Graphite	Hydrothermal	Absorption of Cr^{6+}	The maximum adsorption reached 935 mg g^{-1} in neutral pH at 40 min	127
GQD/Bi_2MoO_6	Graphene sheets	Chemical oxide	CIP/BPA/MB/TC/RhB/simulated solar	90%/90 min/RhB 65%/30 min/TC 75%/30 min/MB 69%/30 min/BPA 80%/30 min CIP 90%/30 min/phenol	128
Ti^{3+}-TiO_2/GQDs NSs	Citric acid	Hydrothermal	Photodegradation of MB and RhB dye	The efficiency of photocatalysis was improved in the nanocomposite compared to TiO_2	129
GQD/mpg-C_3N_4	Pyrene	Hydrothermal	Photodegradation of RhB and TC	UV light, a combination of 0.5 wt% GQD/mpg-C_3N_4 was able to attain a maximum removal efficiency of 97% for RhB. Additionally, the composites were successful in eliminating colorless organic pollutants TC	130

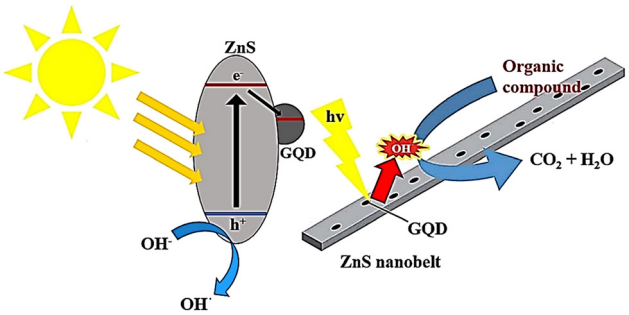

Fig. 11 A possible breakdown process of an organic dye on G/ZnS nanocomposites when exposed to light. Reproduced with permission from ref. 33. Copyright (2016) Royal Society of Chemistry.

In a study, $NiFe_2O_4$/HAP/GQDs were synthesized as a nanoadsorbent to remove cadmium (Cd^{2+}) from aqueous solution. The optimum conditions for the efficient removal of Cd(II) were as follows: a maximum absorption capacity of 344.83 mg g^{-1} at 25 °C and pH = 6.0.[135] A novel, efficient and inexpensive adsorbent based on GQDs coated on quartz sand (GQDs|QS) for the removal of Hg(II) and Pb(II) from aqueous solutions was reported. The maximum adsorption capacity of GQDs|QS for Hg(II) and Pb(II) was calculated to be 24.65 and 24.92 mg g^{-1}, respectively, revealing more improved adsorption capacitance of the GQDs|QS in comparison with nontreated QS. The results show that the particle size of GQDs could influence the removal efficiency of the heavy metals and GQDs with a

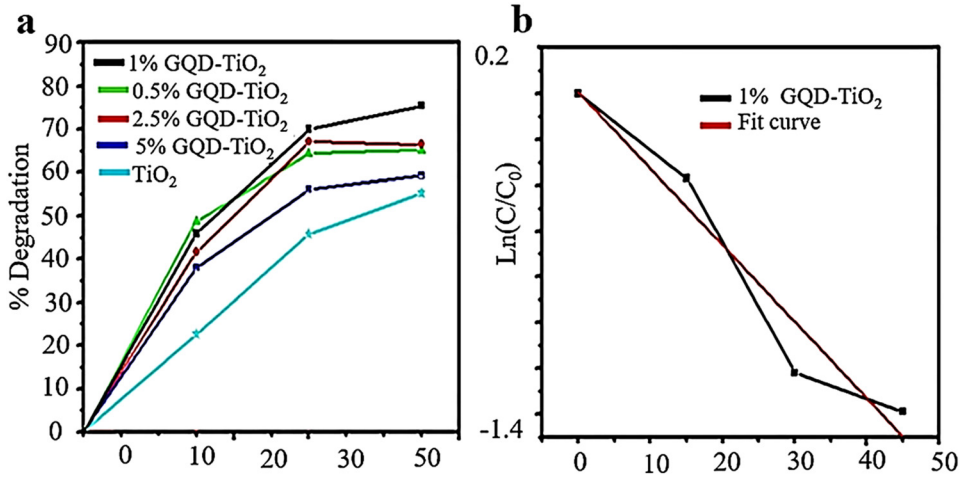

Fig. 12 Photocatalytic degradation of MB *via* TiO_2–GQD composite samples (a) and fitting curve of the first-order kinetic model for 1% TiO_2–GQD composites (b). Reprinted with permission from ref. 133. Copyright (2022) Springer Nature.

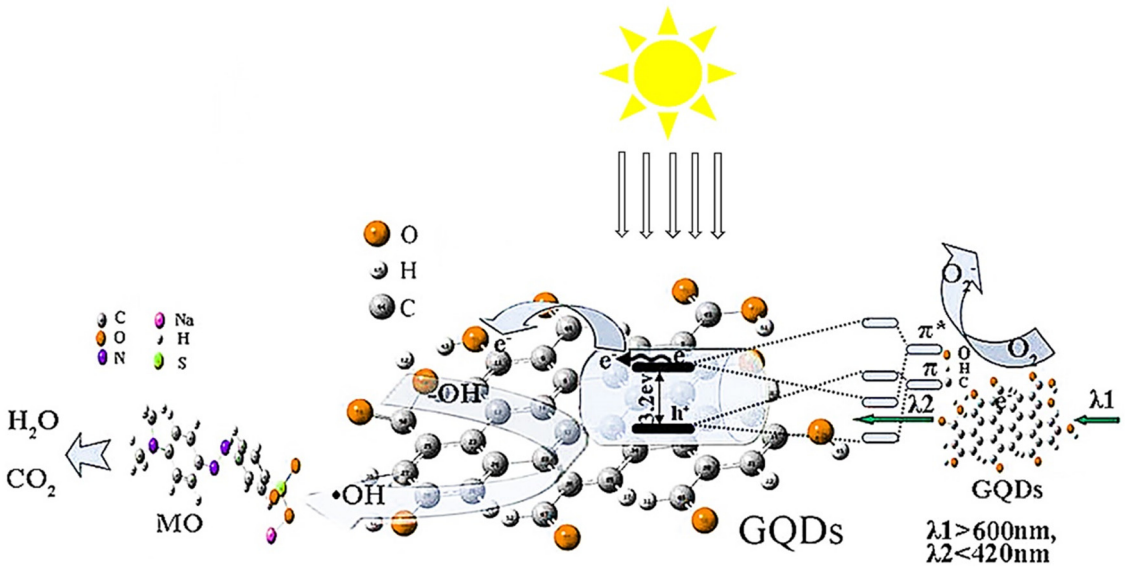

Fig. 13 The schematic of the improved light-driven photocatalysis of GQD/TiO_2-NT composites. Reproduced with permission from ref. 110. Copyright (2016) Elsevier.

carbonization time of 30 min represented the highest removal percentage.[136]

In another study, GQDs were covalently immobilized onto the $NiFe_2O_4$-halloysite nanotube ($NiFe_2O_4$-HNTs) surface to fabricate a nanocomposite material utilized as an active adsorbent to eliminate Pb(II) ions from water. The amount of every independent parameter was determined such that a maximum lead removal of 97.14% could be achieved. The Langmuir isotherm was picked as the best isotherm model for the explanation of lead(II) adsorption. The utmost adsorptive capability was computed as 42.02 mg g^{-1} at 298 K based on the Langmuir mode. The calculated thermodynamic variables exhibited that the uptake operation is heat-absorbing and spontaneous. Therefore, the $NiFe_2O_4$/HNTs/GQDs nano-adsorbent provides an economical and efficient way for eliminating Pb(II) ions.[137]

In a study, GQDs were synthesized *via* pyrolysis and embedded into bacterial cellulose nanopaper (BCN) to develop a well-ordered multi-layered GQD embedded BCN-based filtration membrane assembly for the removal of heavy metal and industrial dye wastewater. The multi-layered GQD embedded BCN-based filtration membrane assembly purified the dye industrial wastewater and selectively eliminated Hg(II) and Pb(II) with efficiencies as high as 99.6% and 97%, respectively.[138]

In another study, Vatanpour *et al.* focused on the use of graphene quantum dots (GQDs) for creating a nanofiltration membrane for removing Reactive Blue 19 dye from wastewater. By adding 1 wt% GQDs to the PVC matrix, the water flux of the membrane increased by 56% compared to the unfilled membrane, reaching 19.1 L m^{-2} h^{-1}. The anti-fouling performance of the membrane was also improved, with a flux recovery ratio increasing from 68.8% to 80.0%. Additionally, all of the PVC membranes fabricated in this study exhibited BSA rejection of more than 98% and Reactive Blue 19 dye rejection of more than 96%. This research demonstrates that the incorporation of GQDs not only enhances permeability but also improves anti-fouling properties without compromising the membrane's rejection performance.[24]

In this study, rice husk was used as a sustainable source to synthesize GQDOs with 2D morphology. Chemical modification of GQDOs with $Ba(OH)_2$ was performed to form a novel GQDOs-Ba nanobiosorbent with an increased number of surface hydroxyl groups. The adsorption parameters of Pb(II) and La(III) onto GQDOs-Ba were optimized using a microwave sorption approach. The maximum capacity reached 3400 μmol g^{-1} (pH = 7), and 1500 μmol g^{-1} (pH = 5) at 15 s for Pb(II) and La(III), respectively. The GQDOs-Ba nanobiosorbent accomplished excellent removal percentages from different water samples containing lead (98.5%–99.8%) and lanthanum (94.6%–96.2%).[101]

Maia *et al.* synthesized a selective and low-cost adsorbent for Hg(II) by functionalizing σ-FeOOH nanoparticles with L-cysteine (cys-σ-FeOOH). cys-σ-FeOOH was highly selective for Hg(II) adsorption because Hg could be complexed with sulfur. Accordingly, the Hg(II) adsorption was determined using the Langmuir isotherm. The Hg(II) adsorption provided by the Langmuir isotherm for cys-σ-FeOOH (217 mg g^{-1}) was significantly higher than that of σ-FeOOH (135 mg g^{-1}).[139]

In another study, ionic liquids (ILs) with liquid ion coatings were used as a new absorbent for removing heavy metal ions, specifically chromium(VI). ILs are considered highly effective solvents for liquid–liquid extraction and heavy metal ion absorption due to their strong electrostatic attraction resulting from polar functions, high adjustability and solubility, ease of operation, and compatibility with the environment. The IL-GQD absorbent demonstrated rapid removal of Cr^{6+} from an aqueous solution. The maximum absorption reached 934.62 mg g^{-1} in 40 minutes under neutral conditions. The effects of external ions on the absorption of Cr^{6+} are illustrated in Fig. 14a, which shows that competing cations had no significant effect on chromium absorption by the prepared absorbents. This may be because the absorption operation was accomplished at a neutral pH, causing the surface of the absorbent to become protonated, leading to repulsion between competing cations and positive surfaces under acidic conditions. Anions, for example, NO^{3-}, SO_4^{2-}, and Cl^-, had a slight effect on chromium absorption. The IL-GQD absorbent has a good absorption capacity compared to other absorbents, such as GO, GQD, and IL-GO.[127] Regeneration investigations were conducted using a base medium as a washing solution. Fig. 14b shows that each GQD, IL-GQD, GO, and IL-GO absorbent can be successfully utilized while maintaining an efficiency removal rate of over 80% for up to five cycles.[11] The mechanism of chromium adsorption due to charge in the IL-GQD adsorbent is shown in Fig. 14c. IL GQD induces imidazole ionic liquid, –NHCO– bonds, and –OH functions. The protonated amine arranges itself with its long chain towards the molecule's periphery, causing the NH^+ portions to interact electrostatically with the hexavalent chromium oxonium. Due to the protonation of the ionic liquid portions, carboxylic acid groups, and amide bonds, the IL-GQD adsorbent does not react and acquires positive charges at neutral to low pH. Due to strong electrostatic interactions between IL-GQD and chromate oxonium groups, the absorption rate increases.[127]

GQDs, as a newcomer in the carbon family of nanofluorescents, are used for several metal ions due to their optical probing.[94] Abbas and colleagues synthesized GQDs which were in the range of 5–20 nm and showed independent PL emission from stimulation. This phenomenon is attributed to the unique fluorescence center of these GQDs. These GQDs are utilized for sensitive measurements and highly selective for Fe^{3+}. A sensitive sensor was obtained for the selective detection of Fe^{3+} with a detection limit of less than 2.5×10^{-6} M.[140] The fluorescence intensity of N-GQDs at various pH values is depicted in Fig. 16. The initial pH value of N-GQDs is 8, as illustrated in Fig. 15. The fluorescence intensity reduces as the pH value decreases, and it reaches its minimum at pH = 5. Conversely, the fluorescence intensity gradually decreases as the pH value increases. Therefore, it can be inferred that N-GQDs can withstand strong alkaline conditions but not strong acidic conditions.[133]

Recently, fluorescent probe explorers have studied metal ions using fluorescent probes, or GQDs, doped with other elements such as nitrogen, sulfur, and phosphorus.[141,142] Elemental doping changes the PL properties of GQDs, and all N/S/P-doped GQDs have better quantum performance than undoped GQDs.[143] A study

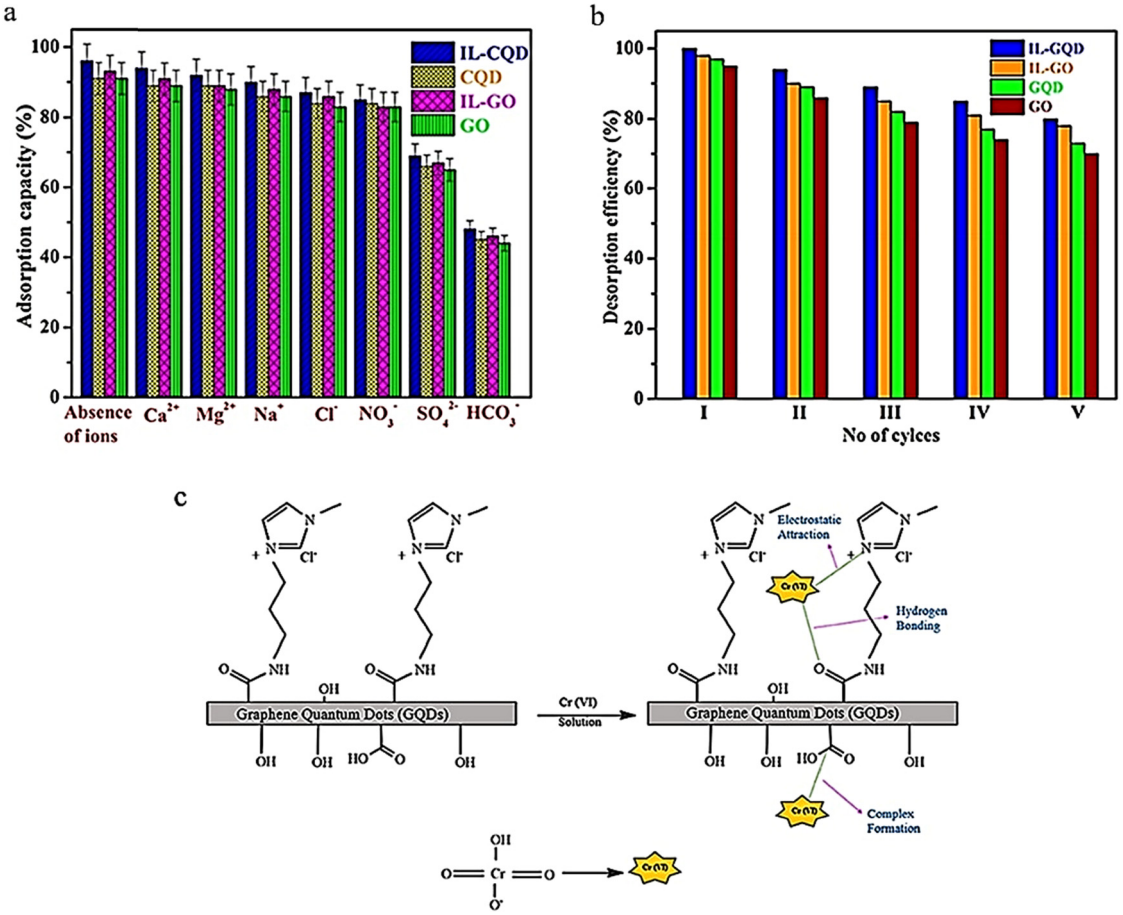

Fig. 14 Effect of competing Cr^{6+} ion adsorption with adsorbents GQD and IL-GQD (a), desorption of the adsorbents IL-GO, IL-GQD, GO, and GQD (b), and acceptable Cr^{6+} adsorption mechanism of the IL-GQD adsorbent (c). (a) and (c) Reprinted with permission from ref. 127 Copyright (2019) American Chemical Society. (b) Reprinted with permission from ref. 11. Copyright (2021) Elsevier.

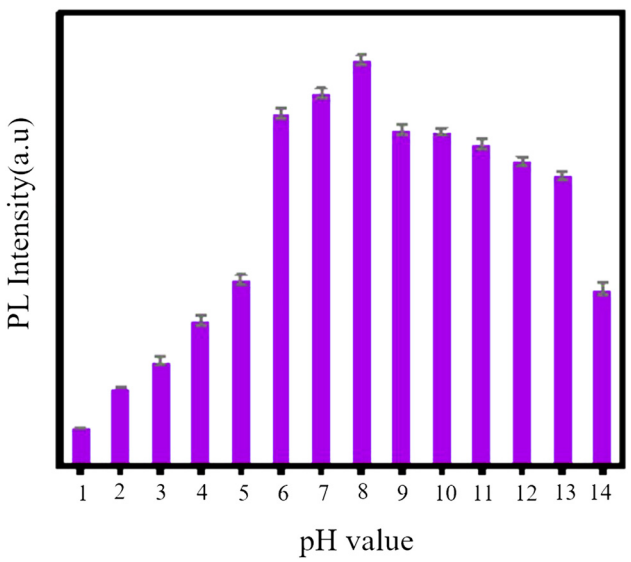

Fig. 15 Fluorescence intensity of N-GQDs at different pH values. Adapted with permission from ref. 133. Copyright (2022) MDPI.

introduced a fluorescent probe highly selective for Hg^{2+} and utilized N-GQDs. These dots are nearly spherical, have an average diameter of 2.7 nm, and emit independently of stimuli. The probes' ability to measure Hg^{2+} was evaluated through a PL-dependent emission spectrum. Hg^{2+} was found to quench the fluorescence of N-GQDs both dynamically and statically. This probe has a broad detection range (2.5–800 mM) and a detection limit of 2.5 mM, making it effective in determining the amount of Hg^{2+} in water samples.[144] To assess the ability of N-GQDs for detecting Cu^{2+} in water, PL properties of N-GQD solutions with varying concentrations of Cu^{2+} were measured using an excitation wavelength of 365 nm. Fig. 16 shows that as the concentration of Cu^{2+} increases, there is a noticeable decrease in PL intensity.[145] A new method has been developed for detecting Cr^{6+} in environmental water samples using N-GQDs, which are selective towards Cr^{6+}. This makes them a valuable and environmentally friendly sensor platform for detecting Cr^{6+} ions in aqueous solutions and natural water samples without labeling. Compared to N-GQDs, GQDs have significantly improved selectivity for detecting Cr^{6+}. The fluorescent probe N-GQDs can detect Cr^{6+} in concentrations ranging from 0–140 mM with a detection limit of 40 nM.[146]

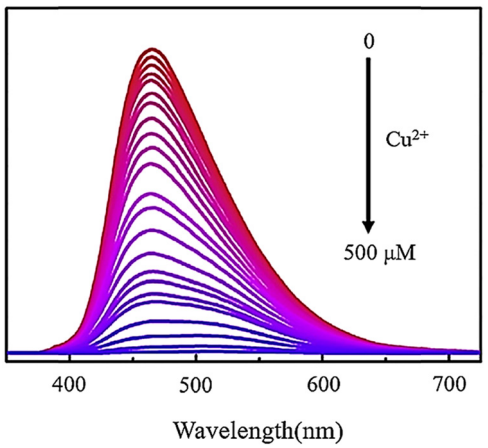

Fig. 16 Fluorescence spectra of N-GQDs, including Cu^{2+} with different concentrations from 0 to 500 μM. Reprinted with permission from ref. 145. Copyright (2020) Elsevier.

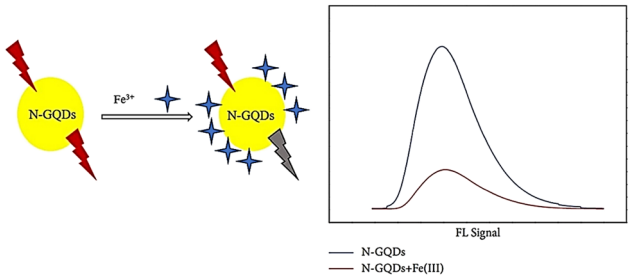

Fig. 17 Quenching N-GQD fluorescence with iron ions. Reproduced with permission from ref. 147. Copyright (2019) Hindawi.

A study was conducted where N-GQDs were synthesized *via* a hydrothermal treatment using ethylenediamine and citric acid as sources of nitrogen and carbon, respectively. These N-GQDs exhibited blue solid fluorescence and a high QY of over 88.9%. The blue fluorescence emission was not affected by excitation wavelengths. As shown in Fig. 17, N-GQDs were employed as fluorescent probes for detecting iron ions, and they showed good sensitivity with a detection limit of 2.37 μmol L^{-1} and a linear range of 1600–6000 μmol L^{-1} for Fe^{3+}.[147]

Another study examined N,S-GQDs that are selective and sensitive for detecting Hg^{2+} in H_2O and wastewater at the nanomolar level. The results displayed in Fig. 18a indicate that the fluorescence intensity remains unchanged when other metal ions are added. However, a significant decrease is observed when Hg^{2+} is introduced to the measurement solutions.[148] Furthermore, the concentration can be obtained from the Stern–Volmer equation:

$$\frac{I}{I_0} = 1 + k_{sv}[Q]$$

where I_0 and I are the fluorescence intensities of GQDs before the presence of metal ions, Q is the quencher concentration (mMol L^{-1}), and k_{sv} is the Stern Volmer constant after the presence of metal ions.[149] Therefore, the I/I_0 ratio obtained for Hg^{2+} was lower than those for other metals. Fig. 18b shows changes in fluorescence intensity of N,S-GQDs after adding different concentrations of Hg^{2+} from 1 nM–15 mM. The fluorescence intensity of N,S-GQDs reduces on enhancing the Hg^{2+} concentration, and 90% of initial fluorescence intensity is quenched at 15 mM Hg^{2+}.[148]

The application of GQDs in wastewater treatment

Several studies have offered the use of GQDs in wastewater treatment or monitoring. For example, GQDs are used for monitoring hazardous substances in industrial effluents,[150] as well as for uranium removal[151] and 4-nitrophenol removal in water samples.[152]

Wastewater treatment is crucial in water treatment as it guarantees that water is not contaminated with harmful microorganisms. If wastewater is not treated, microorganisms like bacteria, fungi, algae, and viruses can infiltrate the water distribution system. Furthermore, the excessive use of antibiotics has resulted in the emergence of drug-resistant bacteria in

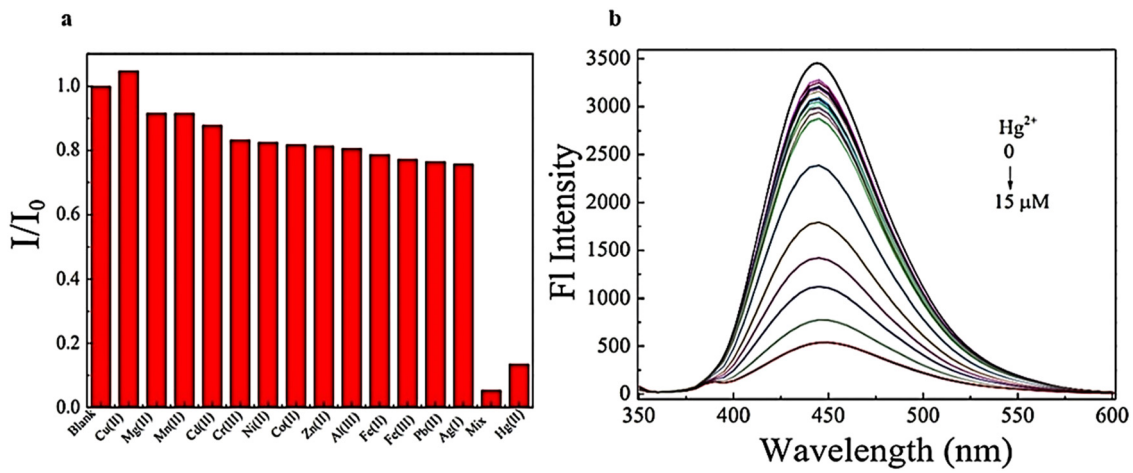

Fig. 18 Emission fluorescence spectra of N,S-GQDs using diverse concentrations Hg^{2+} (0–15 μM) (a) and selectivity of N,S-GQDs using diverse metal ions (b). Reprinted with permission from ref. 148. Copyright (2017) Elsevier.

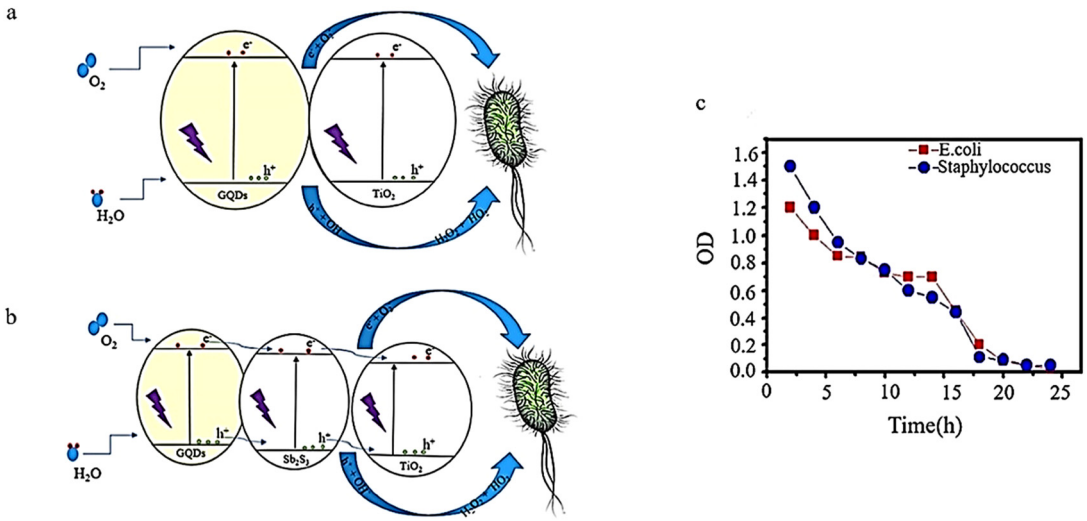

Fig. 19 Bacterial growth inhibition using TiO_2/GQDs (a), TiO_2/Sb_2S_3/GQDs (b), and TiO_2/Sb_2S_3/GQD over one day under visible light (c). (a) and (b) Reproduced with permission from ref. 125. Copyright (2019) Elsevier. (c) Reprinted with permission from ref. 26. Copyright (2020) Elsevier.

the environment. Photocatalytic H_2O disinfection proposes a viable alternative or supplement to chlorination for treating wastewater. As a supplementary procedure, photocatalytic treatment can remove microorganisms and disinfection by-products produced during chlorination.[43]

To examine its ability to destroy bacteria, a GQDs/Sb_2S_3/TiO_2 nanocomposite was created using a solvothermal method. The effectiveness of this composite against two bacterial strains, *E. coli*, and *S. aureus*, was tested. The findings revealed that adding GQDs increased electron–hole pair production (Fig. 19a). As a result, TiO_2/GQD demonstrated superior antibacterial properties compared to pure TiO_2. Empty GQDs had an MIC of 0.5 and 0.1 for *S. aureus* and *E. coli*, respectively.[125]

Adding GQDs to Sb_2S_3 improves its performance through the exact MIC mechanism. Sb_2S_3 exhibits MICs of 0.3 and 0.09 for *Staphylococcus aureus* and *E. coli*, respectively, while Sb_2S_3/GQD shows MICs of 0.2 and 0.07 for *Staphylococcus aureus* and *E. coli*, respectively. Lastly, MICs of 0.03 and 0.1 were obtained for *E. coli* and *Staphylococcus aureus*, respectively. These highest antibacterial properties are due to the ability of Sb_2S_3 and GQD to act as a sensitizer and help TiO_2 produce holes and more electrons (Fig. 19b). The initial stage involves generating pairs of electrons and holes. The electron found in the conduction band can reduce TiO_2, GQDs, and Sb_2S_3 to form superoxide radicals ($^{\bullet}O^{2-}$). Additionally, the holes in the valence band of TiO_2, GQDs, and Sb_2S_3 can interact with H_2O or OH^- adsorbed on the composite surface, creating $^{\bullet}OH$, H_2O_2, and $^{\bullet}HO_2$. Ultimately, the electron–hole pairs produced and active oxygen species formed from their reaction with OH-, H_2O, and O_2 result in bacterial decomposition.[125] As shown in Fig. 19c, there is a decline in bacterial growth as the irradiation period increases until there is almost no growth observed after 24 hours.[43]

In another study, the effect of the shape of oxide nanoparticles on their antimicrobial and photocatalytic virtues was investigated. Zinc oxide (ZnO) nanorods and ZnO nanoflakes were connected to GQDs through coalescence to form ZnO-NRs@GQDs or ZnO-NFs@GQDs nanohybrids, which were tested against *S. aureus*, *P. aeruginosa*, *E. coli*, and *B. cereus*. The results of the zone of inhibition (ZOI) areas are depicted in Fig. 20, where ZnO-NR nanohybrids exhibited better antimicrobial properties and provided better internalization possibilities. The maximum ZOI area for ZnO-NRs@GQDs against *S. aureus* (40 ± 2 mm^2) was observed compared to *E. coli* (37 ± 2 mm^2) for ZnO-NRs@GQDs. On the other hand, the minimum inhibitory area for pristine ZnO-NRs against *E. coli* (11 ± 2 mm^2) was tested.[153]

CDs have plenty of hydrophilic carbonyl and carboxyl groups on their surface, which benefits their uniform dispersion in water. In addition, these surface functional groups have an immense tendency to get attached to the pendant polar groups that are present in polymers. Furthermore, these functional groups help in easing the membrane fabrication process while incorporating CDs into polymers and provide better membrane performances.[154] Mixed matrix nanocomposite membranes (MMNMs) are produced by incorporating engineered nanoparticles (ENPs) into the polymer matrix using one of the following techniques: electrospinning, interfacial polymerization (IP), physical coating, phase inversion, self-assembly or *via* layer-by-layer assembly.[155–157]

The exceptional dispersion in water, small size, and high removal efficiency make GQDs a potential nanofiller for thin film composite membranes (TFNs). The hydrophilic GQDs in the nano-ionic phase can significantly enhance the proton conductivity of the membrane. As a result, GQDs are ideal for absorbing water molecules and creating shorter diffusion paths or reducing entanglement in membranes. This is due to their small pore size, which is suitable for producing nanocomposite membranes with desirable water permeability.[158,159] The removal efficiency of the composite membrane depends on (a) membrane

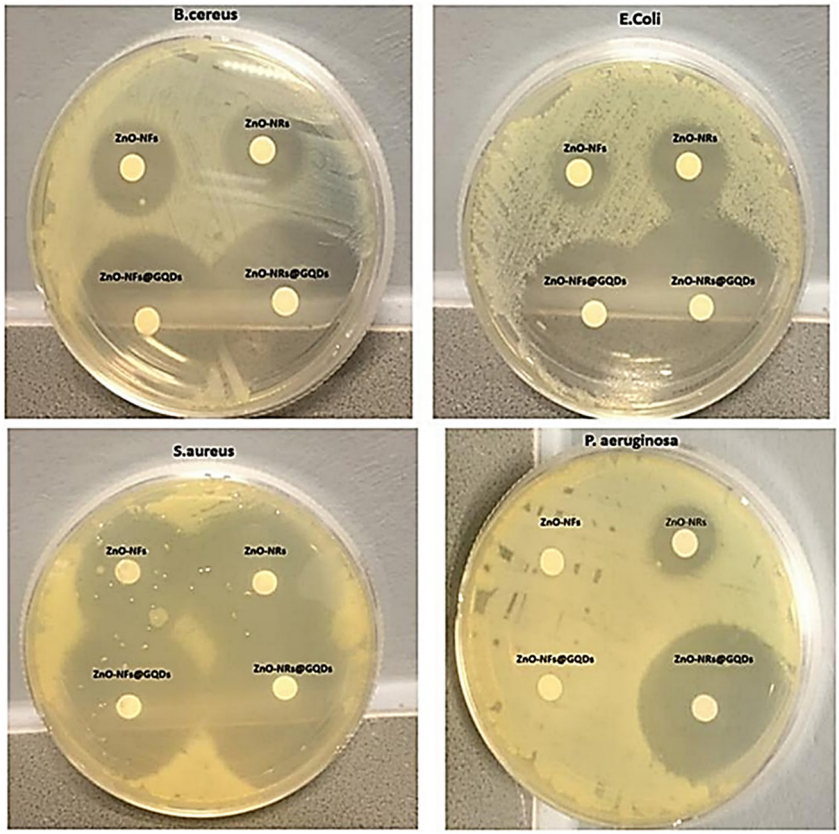

Fig. 20 Inhibitory effect of ZnO-NFs, ZnO-NRs, ZnO-NRs@GQD, and ZnO-NFs@GQD on Mueller Hinton agar plates tested against *S. aureus*, *E. coli*, *B. cereus*, and *P. aeruginosa*. Reprinted with permission from ref. 153. Copyright (2020) Elsevier.

functioning properties such as transmembrane pressure and water flux; (b) membrane characteristics including the size of the pores size, surface charge, and hydrophobicity; and (c) the emerging physicochemical features of the pollutant (*e.g.*, polarity, charge, size, and solvency).[160]

In a study, TFN membranes were produced with GQDs to increase water permeability and anti-fouling properties.[161] TFN membranes were made with 2 nm GQDs through piperazine IP and trimesoyl chloride. GQDs were added to the membranes as aqueous additives. For the supporting membrane, poly(ether sulfone) was added. The addition of small GQDs effectively regulated the structure of the membrane, the roughness of the surface, and the water resistance of the formed TFN membranes.[154] In this study, the anti-fouling properties of the produced membranes were evaluated using humic acid (HA), bovine serum albumin (BSA), and oil emulsion as model fouling agents in a dead-end filtration test. Time-dependent water fluxes are plotted in Fig. 21. During the filtration of fouling solutions, due to the adsorption and deposition of foulants on membrane surfaces, water flux had a rapid decline.[161] The flux of the GQDs/PIP-TMC TFN membrane (3#) declined more sharply than that of the PIP-TMC NF membrane (0#) due to the concentration polarization caused by high flux. After a certain period of operation time, the flux tended to stabilize. This could be interpreted from the dynamic equilibrium of the foulant adsorption.[161] The results showed

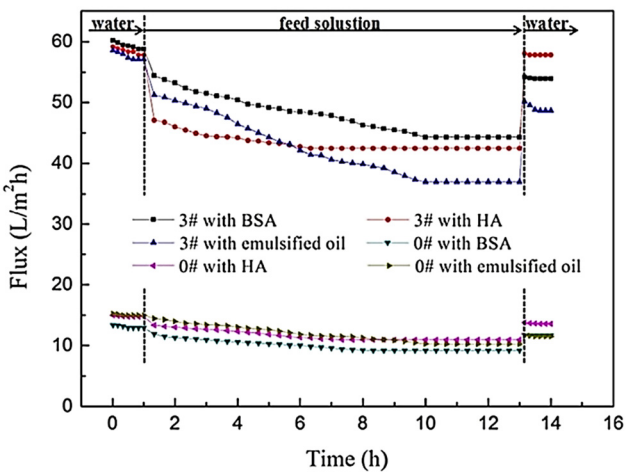

Fig. 21 The time-dependent flux of the PIP-TMC NF membrane (#0) and the GQD/PIP-TMC TFN membrane (#3) during the filtration of HA, BSA, and emulsified oil solutions.[161] Reprinted with permission from ref. 161 Copyright (2018) Elsevier.

that polyamide GQD-TFN membranes can achieve constant water flux under severe fouling conditions.[154]

Polymerization of GQDs and TMC was used for engineering nanofiltration membranes through ultrafiltration (UF) membrane pores and thermal treatment. After engineering the GQD pores,

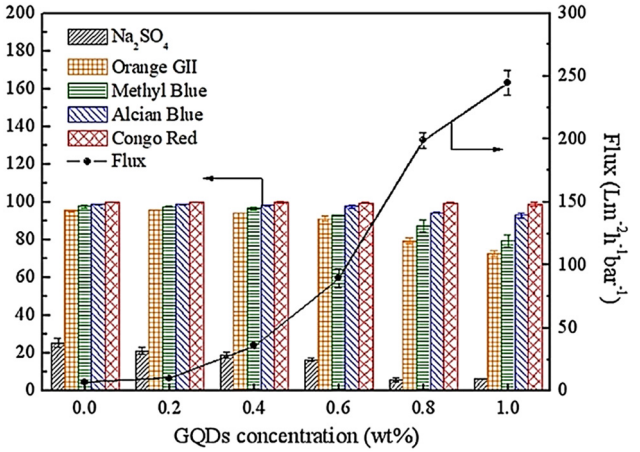

Fig. 22 Water flux and dyes removal percentage for PVC/GQD membranes. Reprinted with permission from ref. 162. Copyright (2019) Elsevier.

many GQD nanoclusters in UF membrane pores can control the UF membrane contraction during thermal treatment so that water flux increases significantly with increasing pore diameter (Fig. 22). Integration of GQD nanoparticles into the membrane structure with a loose surface structure provides additional pathways for increasing permeate flux. The cavities between GQD nanoclusters with smooth and frictionless surfaces transform water transfer channels through PES/GQDs-TMC NF membranes, and the size of nano-channels increases with the increasing amounts of GQDs.[162] The results showed that the NF membrane improved water flux and rejection attributes for alcian blue (AB), orange II (OGII), and congo red (CR), while Na_2SO_4 enhanced it. The rejection rates for AB and CR were more than 90%, which could be due to the physical separation *via* membrane nano-channels and potential repulsive forces between the dye molecules and the membrane surface. The study found that increasing GQDs from 0.6 to 0.1 wt% led to a reduction in OGII and MB rejection rates from 91.2 to 72.6% and 92.2 to 79.4%, respectively.[43]

Vatanpour and colleagues have investigated the potential use of GQDs as a water-friendly nanofiller to enhance PVC-based nanofiltration membranes. The water-friendliness of the membrane improved with increasing amounts of GQDs due to the presence of functional groups on the surface of GQDs, which also helped improve permeability. Additionally, adding GQDs can help increase color absorption in the membrane matrix. However, the results showed that color fading in PVC membranes mixed with prepared GQDs did not improve. Nevertheless, properties such as anti-fouling and permeability improved color removal ability, resulting in high membrane efficiency.[113]

Conclusion and outlook

GQDs provide a possible solution for combating pollutants that contaminate drinking water resources. Water treatment plants must utilize cost-effective, sustainable, and environmentally friendly technologies. All of these features are compatible with GQDs. To make GQDs, raw materials such as graphite, ascorbic acid, citric acid, carbohydrates, plant sources, glucose, lignin waste, fruits, and ammonium citrate are used. However, the production of GQDs from sustainable materials should be encouraged due to their cost-effectiveness, widespread availability, low toxicity, and environmental compatibility. GQDs can be obtained using various artificial methods, with the hydrothermal method being the most popular choice due to its low energy consumption, low cost, and one-step preparation. Despite requiring a long heating time of 8 to 12 hours, this method does not necessitate any purification procedure as the resulting product is highly pure and water-soluble. This review article assesses the potential of GQDs for wastewater treatment owing to their excellent biocompatibility, strong fluorescent effect, high photochemical stability, and low toxicity. Incorporating GQDs into nanocomposites has led to improved efficiency in removing various pollutants. GQDs have also been used in membrane technology either by embedding into membranes or by covalently linking to polymers. Incorporation of GQDs into the membrane matrix improves the efficiency of the treatment of dyes, the membrane characteristics, and their antimicrobial properties. The antimicrobial properties of GQDs could be exploited further in the disinfection of wastewater as an alternative step to chlorination. GQDs have also been evaluated in the adsorption of heavy metals in wastewater. Companies must have accurate management and enhancement of GQD quantities to guarantee their effectiveness in eliminating pollutants in various nanocomposites. Although there have been encouraging developments in GQD-based nanostructures, further efforts are necessary to ensure the creation and employment of these substances in extensive usage. Industrial methods have not yet been able to produce GQDs with uniform size and surface performance, and creating synthetic pathways that ensure appropriate distribution in the nanocomposite matrix remains a challenge. Once these restrictions are addressed, the full potential of GQD utilization for wastewater treatment can be fully realized.

Abbreviations

GQD	Graphene quantum dot
ILs	Ionic liquids
QD	Quantum dot
CA	Citric acid
AB	Alcian blue
QY	Quantum yield
TC	Tetracycline
BPA	Bisphenol A
MO	Methyl orange
MWCNTs	Multiwall carbon nanotubes
HA	Humic acid
UV	Ultraviolet
BCN	Bacterial cellulose nanopaper
CF	Carbon fiber
CNTs	Carbon nanotubes

TMC	Trimesoyl chloride
Bf	Bamboo timber waste
NTs	Nanotubes
mpg-C_3N_4	Mesoporous graphitic carbon nitride
EFB	Empty fruit bunches
GO	Graphene oxide
DMF	*N*,*N*-Dimethylformamide
PL	Photoluminescence
CR	Congo red
OGII	Orange II
PLA	Pulsed laser ablation
UF	Ultrafiltration
MIC	Minimum inhibition concentration
RhB	Rhodamine B
PEI	Polyethylenimine
BSA	Bovine serum albumin
AFB_1	Aflatoxin B_1
QS	Quartz sand
NF	Nanofiltration
TFN	Thin film nanocomposite
ZOI	Zone of inhibition
PLAL	Pulsed laser ablation liquid
NPs	Natural waste precursors
N-GQDs	Nitrogen-doped graphene quantum dots
OPEFB	Oil palm empty fruit bunches

Author contributions

P.G. Balkanloo: writing – original draft, conceptualization, resources, and validation; K.M. Sharifi: writing – original draft, investigation, and visualization; A.P. Marjani: supervision, data curation, editing draft, and project administration.

Conflicts of interest

The authors declare no conflicts of interest.

Acknowledgements

The authors are grateful to Urmia University for supporting this research.

References

1 D. Bera, L. Qian, T.-K. Tseng and P. H. Holloway, *Materials*, 2010, **3**, 2260–2345.
2 X. Guan, Z. Li, X. Geng, Z. Lei, A. Karakoti, T. Wu, P. Kumar, J. Yi and A. Vinu, *Small*, 2023, **19**, 2207181.
3 S. Dorontić, S. Jovanović and A. Bonasera, *Materials*, 2021, **14**, 6153.
4 M. Bacon, S. J. Bradley and T. Nann, *Part. Part. Syst. Charact.*, 2014, **31**, 415–428.
5 S. Zhou, H. Xu, W. Gan and Q. Yuan, *RSC Adv.*, 2016, **6**, 110775–110788.
6 J. Soleymani, M. Hasanzadeh, M. H. Somi, S. A. Ozkan and A. Jouyban, *Int. J. Biol. Macromol.*, 2018, **118**, 1021–1034.
7 S. Kundu and V. K. Pillai, *Phys. Sci. Rev.*, 2020, **5**, 20190013.
8 J. Shen, W. Chen, Z. Yang, G. Lv, J. Cao, D. Li and X. Liu, *NANO*, 2021, **16**, 2130001.
9 Z. Liu, F. Li, Y. Luo, M. Li, G. Hu, X. Pu, T. Tang, J. Wen, X. Li and W. Li, *Molecules*, 2021, **26**, 3922.
10 S. Hu, J. Liu, X. Luo, Q. Shen, Y. Qin, H. Hu, J. Yuan, S. Chen and D. Xu, Available at SSRN: **https://dx.doi.org/10.2139/ssrn.4355156**.
11 C. S. Tshangana, A. A. Muleja, A. T. Kuvarega, T. J. Malefetse and B. B. Mamba, *J. Water Process. Eng.*, 2021, **43**, 102249.
12 A. Kalluri, D. Debnath, B. Dharmadhikari and P. Patra, in *Methods in Enzymology*, ed. C. V. Kumar, Academic Press, 2018, vol. 609, pp. 335–354.
13 P. Tian, L. Tang, K. S. Teng and S. P. Lau, *Mater. Today Chem.*, 2018, **10**, 221–258.
14 F. F. Habibah, A. L. Ivansyah, S. Ivan and R. Hertadi, *RSC Adv.*, 2023, **13**, 2949–2962.
15 H.-A. S. Tohamy, N. A. Fathy, M. El-Sakhawy and S. Kamel, *Diamond Relat. Mater.*, 2023, **132**, 109640.
16 S. A. I. S. M. Ghazali, I. Fatimah, Z. N. Zamil, N. N. Zulkifli and N. Adam, *Open Chem.*, 2023, **21**, 20220285.
17 M. Valian, F. Soofivand, A. Khoobi, Q. A. Yousif and M. Salavati-Niasari, *Arabian J. Chem.*, 2023, **16**, 104401.
18 H. R. Rajabi, O. Khani, M. Shamsipur and V. Vatanpour, *J. Hazard. Mater.*, 2013, **250–251**, 370–378.
19 R. Wang, H. Fan, W. Jiang, G. Ni and S. Qu, *Appl. Surf. Sci.*, 2019, **467–468**, 446–455.
20 Y. Dong, J. Shao, C. Chen, H. Li, R. Wang, Y. Chi, X. Lin and G. Chen, *Carbon*, 2012, **50**, 4738–4743.
21 P. Nuengmatcha, *Environ. Processes*, 2021, **8**, 1289–1306.
22 M. E. Mahmoud, N. A. Fekry and A. M. Abdelfattah, *J. Ind. Eng. Chem.*, 2022, **115**, 365–377.
23 M. E. Mahmoud, N. A. Fekry and S. M. S. Mohamed, *J. Water Process. Eng.*, 2022, **46**, 102562.
24 V. Vatanpour, S. S. Mousavi Khadem, M. Masteri-Farahani, N. Mosleh, M. R. Ganjali, A. Badiei, E. Pourbashir, A. H. Mashhadzadeh, M. Tajammal Munir, G. Mahmodi, P. Zarrintaj, J. D. Ramsey, S.-J. Kim and M. R. Saeb, *J. Water Process. Eng.*, 2020, **38**, 101652.
25 N. Sarkar, G. Sahoo and S. K. Swain, *J. Mol. Liq.*, 2020, **302**, 112591.
26 G. Mamba, L. Moss, G. Gangashe, S. Thakur, V. Muthuraj, S. Vadivel, G. D. Vilakati and T. T. I. Nkambule, in *Micro and Nano Technologies, Carbon Nanomaterials for Agri-Food and Environmental Applications*, ed. K. A. Abd-Elsalam, Elsevier, 2020, pp. 193–215, DOI: **10.1016/B978-0-12-819786-8.00010-4**.
27 W. Liu, C. Ning, R. Sang, Q. Hou and Y. Ni, *Ind. Crops Prod.*, 2021, **171**, 113963.
28 S. Benítez-Martínez and M. Valcárcel, *TrAC, Trends Anal. Chem.*, 2015, **72**, 93–113.
29 C. Erkmen, Y. Demir, S. Kurbanoglu and B. Uslu, *Sens. Actuators, B*, 2021, **343**, 130164.

30 M. K. Chini, V. Kumar, A. Javed and S. Satapathi, *Nano-Struct. Nano-Objects*, 2019, **19**, 100347.
31 J. Shen, Y. Zhu, X. Yang and C. Li, *Chem. Commun.*, 2012, **48**, 3686–3699.
32 D. Iannazzo, C. Espro, C. Celesti, A. Ferlazzo and G. Neri, *Cancers*, 2021, **13**, 3194.
33 S. Ham, Y. Kim, M. J. Park, B. H. Hong and D.-J. Jang, *RSC Adv.*, 2016, **6**, 24115–24120.
34 L. Lazzarin, M. Pasini and E. Menna, *Molecules*, 2021, **26**, 5286.
35 A. Abbas, L. T. Mariana and A. N. Phan, *Carbon*, 2018, **140**, 77–99.
36 H. Bhardwaj, C. Singh, R. K. Kotnala and G. Sumana, *Anal. Bioanal. Chem.*, 2018, **410**, 7313–7323.
37 Y. Yan, J. Gong, J. Chen, Z. Zeng, W. Huang, K. Pu, J. Liu and P. Chen, *Adv. Mater.*, 2019, **31**, 1808283.
38 P. Zheng and N. Wu, *Chem. – Asian J.*, 2017, **12**, 2343–2353.
39 S. Mahalingam, A. Manap, A. Omar, F. W. Low, N. F. Afandi, C. H. Chia and N. A. Rahim, *Renewable Sustainable Energy Rev.*, 2021, **144**, 110999.
40 P. Gozali Balkanloo, M. Mahmoudian and M. T. Hosseinzadeh, *Chem. Eng. J.*, 2020, **396**, 125188.
41 K. Rasoulpoor, A. Poursattar Marjani and E. Nozad, *Environ. Technol. Innovation*, 2020, **20**, 101133.
42 H. Sarreshtehdar Aslaheh, A. Poursattar Marjani and P. Gozali Balkanloo, *J. Polym. Environ.*, 2023, **31**, 3230–3247.
43 G. Mambaa, L. Mossa, G. Gangashea, S. Thakurb, V. Muthurajd, S. Vadivele, G. D. Vilakatif and T. TI, *Carbon Nanomater. Agri-Food Environ. Appl.*, 2019, 193.
44 M. Mahmoudian and P. G. Balkanloo, *Iran. Polym. J.*, 2017, **26**, 711–720.
45 M. Mahmoudian, P. G. Balkanloo and E. Nozad, *Chin. J. Polym. Sci.*, 2018, **36**, 49–57.
46 M. Mahmoudian, Y. Khazani, P. Gozali Balkanloo and M. Enayati, *Polym. Bull.*, 2021, **78**, 4313–4332.
47 I. Mohammadi Dehcheshmeh, M. Frediani, A. Poursattar Marjani and P. Najafi Moghadam, *J. Polym. Environ.*, 2023, DOI: **10.1007/s10924-023-02907-w**.
48 A. Amari, N. Elboughdiri, D. Ghernaout, R. H. Lajimi, A. M. Alshahrani, M. A. Tahoon and F. B. Rebah, *Ain Shams Eng. J.*, 2021, **12**, 4007–4014.
49 V. Bressi, A. Ferlazzo, D. Iannazzo and C. Espro, *Nanomaterials*, 2021, **11**, 1120.
50 X. Liu, J. Han, X. Hou, F. Altincicek, N. Oncel, D. Pierce, X. Wu and J. X. Zhao, *J. Mater. Sci.*, 2021, **56**, 4991–5005.
51 Ö. Yunus, K. Şifa, İ. DEHRİ and E. Ramazan, *J. Turk. Chem. Soc., Sect. B*, 2019, **2**, 109–120.
52 Z. Wang, J. Yu, X. Zhang, N. Li, B. Liu, Y. Li, Y. Wang, W. Wang, Y. Li and L. Zhang, *ACS Appl. Mater. Interfaces*, 2016, **8**, 1434–1439.
53 M. Thakur, A. Mewada, S. Pandey, M. Bhori, K. Singh, M. Sharon and M. Sharon, *Mater. Sci. Eng., C*, 2016, **67**, 468–477.
54 S. Mahesh, C. L. Lekshmi, K. D. Renuka and K. Joseph, *Part. Part. Syst. Charact.*, 2016, **33**, 70–74.
55 D. S. Ahmed, M. K. Mohammed and S. M. Majeed, *ACS Appl. Energy Mater.*, 2020, **3**, 10863–10871.
56 M. K. Kumawat, M. Thakur, R. B. Gurung and R. Srivastava, *ACS Sustainable Chem. Eng.*, 2017, **5**, 1382–1391.
57 R. S. Tade and P. O. Patil, *Curr. Appl. Phys.*, 2020, **20**, 1226–1236.
58 Y. Yin, Q. Liu, D. Jiang, X. Du, J. Qian, H. Mao and K. Wang, *Carbon*, 2016, **96**, 1157–1165.
59 V. Veeramani, M. Sivakumar, S.-M. Chen, R. Madhu, H. R. Alamri, Z. A. Alothman, M. S. A. Hossain, C.-K. Chen, Y. Yamauchi and N. Miyamoto, *RSC Adv.*, 2017, **7**, 45668–45675.
60 M. K. Kumawat, M. Thakur, R. B. Gurung and R. Srivastava, *Sci. Rep.*, 2017, **7**, 15858.
61 L. F. de Lima, A. d S. M. de Freitas, A. L. Ferreira, C. C. Maciel, M. Ferreira and W. R. de Araujo, *Sens. Actuators Rep.*, 2022, **4**, 100102.
62 R. Hatefi, A. Mashinchian-Moradi, H. Younesi and S. Nojavan, *J. Environ. Health Sci. Eng.*, 2020, **18**, 1531–1540.
63 S. Gu, C.-T. Hsieh, C.-Y. Yuan, Y. Ashraf Gandomi, J.-K. Chang, C.-C. Fu, J.-W. Yang and R.-S. Juang, *J. Lumin.*, 2020, **217**, 116774.
64 Z.-F. Pu, Q.-L. Wen, Y.-J. Yang, X.-M. Cui, J. Ling, P. Liu and Q.-E. Cao, *Spectrochim. Acta, Part A*, 2020, **229**, 117944.
65 S. Bansal, J. Singh, U. Kumari, I. P. Kaur, R. P. Barnwal, R. Kumar, S. Singh, G. Singh and M. Chatterjee, *Int. J. Nanomed.*, 2019, **14**, 809.
66 S. Bak, D. Kim and H. Lee, *Curr. Appl. Phys.*, 2016, **16**, 1192–1201.
67 W. H. Danial, M. Abdullah, M. A. Abu Bakar, M. S. Yunos, A. R. Ibrahim, A. Iqbal and N. N. Adnan, *Opt. Mater.*, 2022, **132**, 112853.
68 A. Suryawanshi, M. Biswal, D. Mhamane, R. Gokhale, S. Patil, D. Guin and S. Ogale, *Nanoscale*, 2014, **6**, 11664–11670.
69 Z. Ding, F. Li, J. Wen, X. Wang and R. Sun, *Green Chem.*, 2018, **20**, 1383–1390.
70 L. Wang, W. Li, B. Wu, Z. Li, S. Wang, Y. Liu, D. Pan and M. Wu, *Chem. Eng. J.*, 2016, **300**, 75–82.
71 A. Abbas, T. A. Tabish, S. J. Bull, T. M. Lim and A. N. Phan, *Sci. Rep.*, 2020, **10**, 1–16.
72 L. Zhou, J. Geng and B. Liu, *Part. Part. Syst. Charact.*, 2013, **30**, 1086–1092.
73 M. Shehab, S. Ebrahim and M. Soliman, *J. Lumin.*, 2017, **184**, 110–116.
74 L. Tang, R. Ji, X. Li, K. S. Teng and S. P. Lau, *Part. Part. Syst. Charact.*, 2013, **30**, 523–531.
75 W. Liu, C. Ning, R. Sang, Q. Hou and Y. Ni, *Ind. Crops Prod.*, 2021, **171**, 113963.
76 E. Montoneri, *Food waste reduction and valorisation: sustainability assessment and policy analysis*, 2017, 79–120.
77 A. R. Hidayu, N. F. Mohamad, S. Matali and A. S. A. K. Sharifah, *Procedia Eng.*, 2013, **68**, 379–384.
78 D. C. Nieves, K. Karimi and I. S. Horváth, *Ind. Crops Prod.*, 2011, **34**, 1097–1101.
79 S. A. Prabhu, V. Kavithayeni, R. Suganthy and K. Geetha, *Carbon Lett.*, 2021, **31**, 1–12.
80 M. C. Biswas, M. T. Islam, P. K. Nandy and M. M. Hossain, *ACS Mater. Lett.*, 2021, **3**, 889–911.

81 M. R. Younis, G. He, J. Lin and P. Huang, *Front. Chem.*, 2020, **8**, 424.
82 N. Nesakumar, S. Srinivasan and S. Alwarappan, *Microchim. Acta*, 2022, **189**, 258.
83 D. B. Shinde and V. K. Pillai, *Chem. – Eur. J.*, 2012, **18**, 12522–12528.
84 C. Zhao, X. Song, Y. Liu, Y. Fu, L. Ye, N. Wang, F. Wang, L. Li, M. Mohammadniaei, M. Zhang, Q. Zhang and J. Liu, *J. Nanobiotechnol.*, 2020, **18**, 142.
85 C. Zhao, X. Song, Y. Liu, Y. Fu, L. Ye, N. Wang, F. Wang, L. Li, M. Mohammadniaei and M. Zhang, 2020.
86 Y. Zhu, G. Wang, H. Jiang, L. Chen and X. Zhang, *Chem. Commun.*, 2015, **51**, 948–951.
87 D. Iannazzo, C. Celesti and C. Espro, *Biotechnol. J.*, 2021, **16**, 1900422.
88 J. P. Naik, P. Sutradhar and M. Saha, *J. Nanostruct. Chem.*, 2017, **7**, 85–89.
89 G.-L. Hong, H.-L. Zhao, H.-H. Deng, H.-J. Yang, H.-P. Peng, Y.-H. Liu and W. Chen, *Int. J. Nanomed.*, 2018, **13**, 4807.
90 H. Lu, W. Li, H. Dong and M. Wei, *Small*, 2019, **15**, 1902136.
91 S. Kang, Y. K. Jeong, K. H. Jung, Y. Son, S.-C. Choi, G. S. An, H. Han and K. M. Kim, *RSC Adv.*, 2019, **9**, 38447–38453.
92 S. R. M. Santiago, T. N. Lin, C. T. Yuan, J. L. Shen, H. Y. Huang and C. A. J. Lin, *Phys. Chem. Chem. Phys.*, 2016, **18**, 22599–22605.
93 Q. Zhuang, Y. Wang and Y. Ni, *Luminescence*, 2016, **31**, 746–753.
94 C. Zhang, Y. Cui, L. Song, X. Liu and Z. Hu, *Talanta*, 2016, **150**, 54–60.
95 P. Tian, L. Tang, K. Teng and S. Lau, *Mater. Today Chem.*, 2018, **10**, 221–258.
96 S. Zhu, J. Zhang, X. Liu, B. Li, X. Wang, S. Tang, Q. Meng, Y. Li, C. Shi and R. Hu, *RSC Adv.*, 2012, **2**, 2717–2720.
97 Ş. Kir, İ. Dehri, Y. Önal and R. Esen, *Luminescence*, 2021, **36**, 1365–1376.
98 A. K. Singh, S. Sri, L. B. Garimella, T. K. Dhiman, S. Sen and P. R. Solanki, *ACS Appl. Bio Mater.*, 2022, **5**, 1179–1186.
99 W. Chen, J. Shen, G. Lv, D. Li, Y. Hu, C. Zhou, X. Liu and Z. Dai, *ChemistrySelect*, 2019, **4**, 2898–2902.
100 P. Kadyan, R. Malik, S. Bhatia, A. Al Harrasi, S. Mohan, M. Yadav, S. Dalal, S. Ramniwas, S. Kumar Kataria and T. Arasu, *J. Nanomater.*, 2023, 2023.
101 M. E. Mahmoud, N. A. Fekry and A. M. Abdelfattah, *Bioresour. Technol.*, 2020, **298**, 122514.
102 M. S. Iyer and I. Rajangam, *Int. J. Energy Res.*, 2022, **46**, 10833–10843.
103 S. Bian, C. Shen, Y. Qian, J. Liu, F. Xi and X. Dong, *Sens. Actuators, B*, 2017, **242**, 231–237.
104 S. Kellici, J. Acord, N. P. Power, D. J. Morgan, P. Coppo, T. Heil and B. Saha, *RSC Adv.*, 2017, **7**, 14716–14720.
105 A. R. Pai, B. S. Sasi, J. Arya and K. Arjun, *IOP Conf. Series: Mater. Sci. Eng.*, 2022, **1219**, 012005.
106 T. Chen, J. Sun, N. Xue, X. Zhang, H. Wang, K. Jiang, T. Zhou and H. Quan, *J. Mater. Chem. A*, 2022, **10**, 10759–10767.
107 C.-T. Hsieh, P.-Y. Sung, Y. A. Gandomi, K. S. Khoo and J.-K. Chang, *Chemosphere*, 2023, **318**, 137926.
108 A. Muthurasu, P. Dhandapani and V. Ganesh, *New J. Chem.*, 2016, **40**, 9111–9124.
109 H. M. Kashani, T. Madrakian, A. Afkhami, F. Mahjoubi and M. A. Moosavi, *Mater. Sci. Eng., B*, 2019, **251**, 114452.
110 A. Qu, H. Xie, X. Xu, Y. Zhang, S. Wen and Y. Cui, *Appl. Surf. Sci.*, 2016, **375**, 230–241.
111 A. Aghamali, M. Khosravi, H. Hamishehkar, N. Modirshahla and M. A. Behnajady, *J. Lumin.*, 2018, **201**, 265–274.
112 S. Kundu and V. K. Pillai, *Phys. Sci. Rev.*, 2019, **5**, 20190013.
113 V. Vatanpour, S. Mousavi Khadem, M. Masteri-Farahani, N. Mosleh, M. Ganjali, A. Badiei, E. Pourbashir, A. Mashhadzadeh, M. Munir and G. Mahmodi, *J. Water Process. Eng.*, 2020, **38**, 101652.
114 J. Peng, W. Gao, B. K. Gupta, Z. Liu, R. Romero-Aburto, L. Ge, L. Song, L. B. Alemany, X. Zhan and G. Gao, *Nano Lett.*, 2012, **12**, 844–849.
115 S. Kundu, R. M. Yadav, T. Narayanan, M. V. Shelke, R. Vajtai, P. M. Ajayan and V. K. Pillai, *Nanoscale*, 2015, **7**, 11515–11519.
116 S. Sarkar, A. Raghavan, A. Giri and S. Ghosh, *ChemistrySelect*, 2021, **6**, 10957–10964.
117 H. Safardoust-Hojaghan and M. Salavati-Niasari, *J. Cleaner Prod.*, 2017, **148**, 31–36.
118 M. Shafaee, E. K. Goharshadi, M. Mashreghi and M. Sadeghinia, *J. Photochem. Photobiol., A*, 2018, **357**, 90–102.
119 T. Fan, Y. Li, J. Shen and M. Ye, *Appl. Surf. Sci.*, 2016, **367**, 518–527.
120 H. Geng, P. Du, Z. Zhang, L. Yao, K. Cao, S. Li and P. Sheng, *Mater. Lett.*, 2018, **214**, 146–149.
121 M. Oves, M. O. Ansari and I. M. I. Ismail, in *Graphene Quantum Dots*, ed. M. Oves, K. Umar, I. M. I. Ismail and M. N. Mohamad Ibrahim, Woodhead Publishing, 2023, pp. 113–132, DOI: 10.1016/B978-0-323-85721-5.00012-1.
122 Y. Deng, L. Tang, C. Feng, G. Zeng, J. Wang, Y. Lu, Y. Liu, J. Yu, S. Chen and Y. Zhou, *ACS Appl. Mater. Interfaces*, 2017, **9**, 42816–42828.
123 M.-L. Hsieh, R.-S. Juang, Y. A. Gandomi, C.-C. Fu, C.-T. Hsieh and W.-R. Liu, *J. Taiwan Inst. Chem. Eng.*, 2022, **131**, 104180.
124 X. Wu, F. Tian, W. Wang, J. Chen, M. Wu and J. X. Zhao, *J. Mater. Chem. C*, 2013, **1**, 4676–4684.
125 H. Teymourinia, M. Salavati-Niasari, O. Amiri and F. Yazdian, *Mater. Sci. Eng., C*, 2019, **99**, 296–303.
126 M. Rastgordani and J. Zolgharnein, *Mater. Sci. Eng., B*, 2023, **290**, 116290.
127 A. Nagaraj, M. A. Munusamy, A. A. Al-Arfaj and M. Rajan, *J. Chem. Eng. Data*, 2018, **64**, 651–667.
128 Y. Hao, X. Dong, X. Wang, S. Zhai, H. Ma and X. Zhang, *J. Mater. Chem. A*, 2016, **4**, 8298–8307.
129 J. Tang, Y. Liu, Y. Hu, G. Lv, C. Yang and G. Yang, *Chem. – Eur. J.*, 2018, **24**, 4390–4398.
130 J. Liu, H. Xu, Y. Xu, Y. Song, J. Lian, Y. Zhao, L. Wang, L. Huang, H. Ji and H. Li, *Appl. Catal., B*, 2017, **207**, 429–437.
131 R. A. Aftab, A. A. P. Khan, M. Ayaz, M. Nazim and A. M. Asiri, in *Graphene Quantum Dots*, Elsevier, 2023, pp. 211–225.

132 S. Chinnusamy, R. Kaur, A. Bokare and F. Erogbogbo, *MRS Commun.*, 2018, **8**, 137–144.
133 W. Li, N. Jiang, L. Zhang, Y. Chen, J. Gao, J. Zhang, B. Yang and J. He, *Molecules*, 2022, **27**, 7844.
134 R. Sahraei, Z. Sekhavat Pour and M. Ghaemy, *J. Cleaner Prod.*, 2017, **142**, 2973–2984.
135 P. Kahrizi, F. S. Mohseni-Shahri and F. Moeinpour, *J. Nanostruct. Chem.*, 2018, **8**, 441–452.
136 R. Mohammad-Rezaei and M. Jaymand, *Environ. Prog. Sustainable Energy*, 2019, **38**, S24–S31.
137 J. Z. Pirhaji, F. Moeinpour, A. M. Dehabadi and S. A. Y. Ardakani, *J. Mol. Liq.*, 2020, **300**, 112345.
138 A. Pandya, K. Shah, H. Prajapati and G. S. Vishwakarma, *Cellulose*, 2021, **28**, 10385–10398.
139 L. F. Maia, R. C. Hott, P. C. Ladeira, B. L. Batista, T. G. Andrade, M. S. Santos, M. C. Faria, L. C. Oliveira, D. S. Monteiro and M. C. Pereira, *Chemosphere*, 2019, **215**, 422–431.
140 A. Abbas, T. A. Tabish, S. J. Bull, T. M. Lim and A. N. Phan, *Sci. Rep.*, 2020, **10**, 21262.
141 Y. Xu, S. Wang, X. Hou, Z. Sun, Y. Jiang, Z. Dong, Q. Tao, J. Man and Y. Cao, *Appl. Surf. Sci.*, 2018, **445**, 519–526.
142 W. Wang, S. Xu, N. Li, Z. Huang, B. Su and X. Chen, *Spectrochim. Acta, Part A*, 2019, **221**, 117211.
143 K. Wang, J. Dong, L. Sun, H. Chen, Y. Wang, C. Wang and L. Dong, *RSC Adv.*, 2016, **6**, 91225–91232.
144 Y. Liu, X. Tang, M. Deng, Y. Cao, Y. Li, H. Zheng, F. Li, F. Yan, T. Lan, L. Shi, L. Gao, L. Huang, T. Zhu, H. Lin, Y. Bai, D. Qu, X. Huang and F. Qiu, *Microchim. Acta*, 2019, **186**, 140.
145 B. Gao, D. Chen, B. Gu, T. Wang, Z. Wang, F. xie, Y. Yang, Q. Guo and G. Wang, *Curr. Appl. Phys.*, 2020, **20**, 538–544.
146 F. Cai, X. Liu, S. Liu, H. Liu and Y. Huang, *RSC Adv.*, 2014, **4**, 52016–52022.
147 F. Lu, Y.-H. Zhou, L.-H. Wu, J. Qian, S. Cao, Y.-f Deng and Y. Chen, *Int. J. Opt.*, 2019, **2019**, 8724320.
148 N. T. N. Anh, A. D. Chowdhury and R.-A. Doong, *Sens. Actuators, B*, 2017, **252**, 1169–1178.
149 T. Anusuya, V. Kumar and V. Kumar, *Chemosphere*, 2021, **282**, 131019.
150 R. Wang, L. Jiao, X. Zhou, Z. Guo, H. Bian and H. Dai, *J. Hazard. Mater.*, 2021, **412**, 125096.
151 J. Ding, X. Zhou, Y. Huang, B. Chen, S. Chen, Y. Jin, Y. Yang, N. Pan, C. Xu, J. Chen and C. Xia, *Appl. Surf. Sci.*, 2022, **583**, 152492.
152 N. T. N. Anh and R.-a Doong, *ACS Appl. Nano Mater.*, 2018, **1**, 2153–2163.
153 C. Tshangana, M. Chabalala, A. Muleja, E. Nxumalo and B. Mamba, *J. Environ. Chem. Eng.*, 2020, **8**, 103930.
154 M. Jani, J. A. Arcos-Pareja and M. Ni, *Molecules*, 2020, **25**, 4934.
155 H. Gao, Y. Sun, J. Zhou, R. Xu and H. Duan, *ACS Appl. Mater. Interfaces*, 2013, **5**, 425–432.
156 T.-H. Bae, I.-C. Kim and T.-M. Tak, *J. Membr. Sci.*, 2006, **275**, 1–5.
157 M. L. Lind, A. K. Ghosh, A. Jawor, X. Huang, W. Hou, Y. Yang and E. M. Hoek, *Langmuir*, 2009, **25**, 10139–10145.
158 Z. Zeng, D. Yu, Z. He, J. Liu, F.-X. Xiao, Y. Zhang, R. Wang, D. Bhattacharyya and T. T. Y. Tan, *Sci. Rep.*, 2016, **6**, 1–11.
159 U. A. Rani, L. Y. Ng, C. Y. Ng and E. Mahmoudi, *Adv. Colloid Interface Sci.*, 2020, **278**, 102124.
160 N. Bolong, A. Ismail, M. R. Salim, D. Rana and T. Matsuura, *J. Membr. Sci.*, 2009, **331**, 40–49.
161 R. Bi, Q. Zhang, R. Zhang, Y. Su and Z. Jiang, *J. Membr. Sci.*, 2018, **553**, 17–24.
162 R. Bi, R. Zhang, J. Shen, Y.-N. Liu, M. He, X. You, Y. Su and Z. Jiang, *J. Membr. Sci.*, 2019, **572**, 504–511.